Automated extraction of meandering river morphodynamics from multitemporal remotely sensed data

Federico Monegaglia[a,b,*], Guido Zolezzi[a], Inci Güneralp[c,d], Alexander J. Henshaw[b], Marco Tubino[a]

[a] *Department of Civil, Environmental and Mechanical Engineering, University of Trento, Via Mesiano 77, 38123, Italy*
[b] *School of Geography, Queen Mary University of London, Mile End Road, London E1 4NS, UK*
[c] *Department of Geography, Texas A&M University, College Station, TX 77843, USA*
[d] *Center for Geospatial Sciences, Applications and Technology (GEOSAT), Texas A&M University, College Station, TX, USA*

Abstract

We introduce PyRIS an automated, process-based software for extracting extensive meandering and anabranching river morphodynamics from multitemporal satellite imagery, including a unique ability to quantify river bars dynamic. PyRIS provides three main computations: (i) detection of planform centerline including complex river patterns, (ii) computation of migration vectors between subsequent centerlines, and (iii) analysis of sediment bars dynamics. PyRIS was validated against several test cases in the Amazon River basin, specifically i) main channel extraction from the anabranching Amazon river, ii) migration analysis following a large cutoff on the Ucayali River and iii) detection of sediment bar migration on the Xingu River. Tests prove the capability of PyRIS to detect the main channel in anabranching structures and chute cutoffs. PyRIS can extract extensive morphodynamic information with unprecedented automation levels and reasonable computational effort (5 hours for 28 Landsat images of a 240km reach of the Xingu River on a 3.20GHz Intel).

Keywords: meandering river, migration rate, multispectral image, sediment

bar, Landsat archive, automated data extraction

1. Introduction

Traditionally, the planform evolution of river meanders has been studied through analytical models (Ikeda et al., 1981; Johannesson & Parker, 1989; Seminara et al., 2001), field data (Leopold & Wolman, 1960; Lewin, 1972; van den Berg, 1995; Brewer & Lewin, 1998; Lewin & Brewer, 2001; Hooke, 2007; Hooke & Yorke, 2011) and numerical models (Howard, 1992; Sun et al., 1996; Asahi et al., 2013; Eke et al., 2014a). Only recently has the power of modern computers and the availability of geospatial imagery made it possible for researchers to investigate meander morphodynamics from remotely sensed data. In this paper we present a process-based software, PyRIS (Python–RIvers from Satellite), which allows for automated extraction of information on meander morphodynamics from multispectral remotely sensed data, by isolating individual physical processes occurring in evolving meander bends.

In the following sections, we provide some fundamental background on meandering river morphodynamics and then discuss the state of art of remote sensing applications in this research field.

1.1. A brief overview on river meander morphodynamics

Meandering is one of the most intriguing and highly dynamic processes occurring in alluvial riverine environments. The process of meandering occurs as freely evolving rivers with curvilinear planforms wander through their floodplains, carving the landscape and reworking its sediments through the mechanisms of river

*Corresponding author
Email address: federico.monegaglia@unitn.it (Federico Monegaglia)

bank erosion and accretion (Edwards & Smith, 2002; Hooke et al., 2011; Hooke, 2003; Leopold & Wolman, 1960; Seminara, 2006). Eventually meandering rivers encounter planform constraints such as bedrock, valley sides or anthropogenic structures which condition their planform development. Large-scale sediment bedforms called point bars usually develop at the inner banks of meander bends (point bars), gently connecting the floodplain with the river bed (Kasvi et al., 2013; Legleiter et al., 2011; Nanson & Hickin, 1983). A steeper slope connects the channel bed to the outer, eroding bank of meander bends, where the flow depth is generally higher, as well as the streamwise velocity (Eke, 2013; Mosselman, 1998). Experimental, analytical and numerical modeling (Kinoshita & Miwa, 1974; Schuurman et al., 2016; Tubino & Seminara, 1990) indicate that unders some conditinos point bars can coexist with alternate migrating bars, which can be viewed as river bed topography waves with scour and deposition patterns that alternate streamwise and spanwise at opposite banks. Alternate bars are shorter in length and migrate downstream whereas point bars do not (Blondeaux & Seminara, 1985; Colombini et al., 1987; Tubino, 1991).

The analysis of sediment bar dynamics in real meandering rivers has received relatively little attention in the past decades compared to their planform dynamics, for which a large body of theoretical and modelling work has been developed (e.g., Zolezzi et al. 2012). However, recent works started addressing the importance of sediment bars in a wide range of morphodynamic studies focused on real rivers, including effects of massive deforestation on sediment dynamics in the Amazon (Latrubesse et al., 2009), influence of point bar development on the mechanisms of meander migration (Eke et al., 2014b; Hooke & Yorke, 2011; van de Lageweg et al., 2014), effects of mid-channel bar development on planform stability and structure of meandering rivers (Luchi et al., 2010a,b), and alternate

bar dynamics in channelised reaches (Adami et al., 2016). Field-based reconstructions of sediment bar dynamics were proposed by Brewer et al. (2000); Gittins (2004) and the impact of sediment bars on river management was analyzed by O'Callaghan et al. (2013).

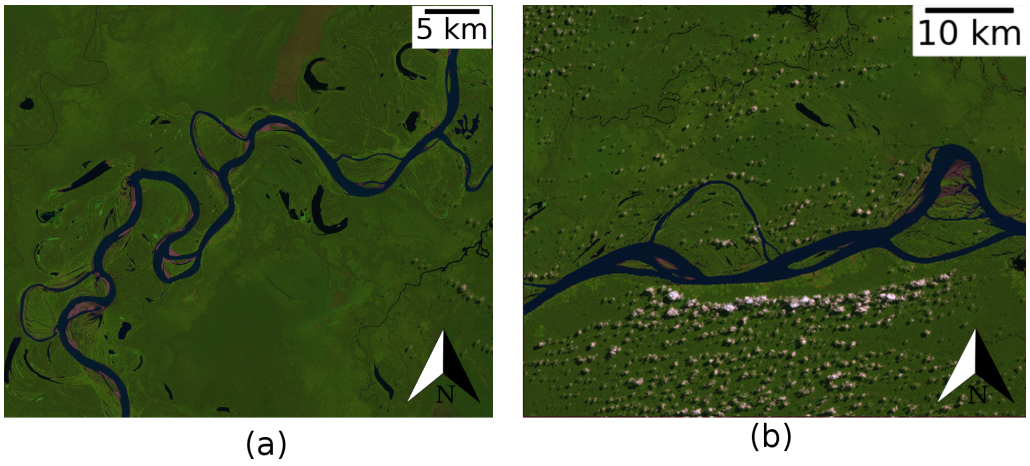

Figure 1: Illustrative examples of river patterns. (*a*) False color map of the meandering Rio Huallaga (Brazil) with chutes. Abandoned meanders (cutoff residuals or oxbow lakes) provide evidence of morphological activity and planform development (Landsat false color composite based on LT05_L1TP_007064_20000730_20161213_01_T1_B(5,4,3).TIF image layers). (*b*) False color map of the anabranching Amazon River (Brazil, Landsat infrared composite based on LT05_L1TP_003062_20010721_20161211_T1_B(5,4,3).TIF image layers).

Meander bends undergo temporal amplification and translation (Eke et al., 2014a; Güneralp & Rhoads, 2009, 2011; Seminara et al., 2001), deformation (Kinoshita, 1961; Schwenk et al., 2015; Seminara et al., 2001) and eventually cutoff processes (Hooke, 2004; Schwenk & Foufoula-Georgiou, 2016) when they grow enough to cut themselves out (neck cutoff, e.g Camporeale et al. (2008), see also figure 1a) or when they are overridden by secondary channels (chute cutoff, e.g. Constantine et al. 2009; Kasvi et al. 2013; Kleinhans & van den Berg 2011). A spatially-distributed indicator of meander planform dynamics is the local migration rate, which represents the local rate of movement of the river centerline

and corresponds to the average between the local rate of erosion of the retreating bank and the local rate of accretion of the advancing one (Eke et al., 2014a,b).

Meandering rivers are commonly viewed as single-thread fluvial patterns, though several transitional styles of meandering actually exist, characterised by the presence of secondary and multiple channels (Figure 1b). Some of the processes described earlier are of particular interest for large meandering rivers. In this study, we also focus on large rivers in the evaluation of PyRIS due to the lack of high spatial resolution data on small rivers spanning long time scales.

In particular, chute cutoffs are one of the dinstinctive characteristics of large active meandering rivers, whereby secondary, chute channels form and connect the upstream and downstram ends of a meander bend thorugh shorter paths that eventually become the main channel after flooding events (Constantine et al., 2010). These transitional meanders may present some similarities with anabranching river systems typical of the largest rivers on Earth like the Amazon river (Latrubesse, 2008), where the main channel splits into multiple sinuous branches which merge together repeatedly in space. The larger a meandering river, the more frequently an anabranching structure is apparent. In fact, the largest rivers on earth are mostly anabraching (Latrubesse, 2008). In contrast to many meandering rivers, anabranching channels are relatively stable in time with a number of channels oscillating in space due to the presence of semi-permanent vegetated islands (Nanson & Knighton, 1996; Carling et al., 2014). The main channel displays very low sinuosities (Amos et al., 2008). According to Nanson & Knighton (1996) anabranching channels are associated with a flow regime that is flood-dominated.

1.2. Remote sensing of river meanders

Most image processing and geospatial analysis tools make it possible to classify and analyse the earth surface through pixel-distributed indices that map vegetation (Carlson & Riziley, 1997), water (Feyisa et al., 2014; Gao, 1996; Xu, 2006; Pai & Saraswat, 2013) and lithology (Ninomiya, 2004). The combination of such indices allows for identifying river and water boundaries in a semi-automated fashion (Güneralp et al., 2013; Güneralp et al., 2014). A number of approaches for the extraction of channel centerlines (Fisher et al., 2013; Schwendel et al., 2015; Schwenk et al., 2016; Schwenk & Foufoula-Georgiou, 2015) and banks (Güneralp et al., 2014; Güneralp et al., 2013; Merwade, 2007; Pavelsky & Smith, 2008; Rowland et al., 2016; Schwenk et al., 2016) from river masks has been developed so far (tools for the extraction of channel planforms from topography data are also available, e.g. Sangireddy et al. 2016). The recently published Rivamap software by Isikdogan et al. (2017) facilitates the delineate of river bodies by applying a singularity index in a fully automated manner; however, their algorithm breaks the connectivity of river reaches, hence it makes it impossible to vectorize the channel centerline. Centerline extraction is generally performed by skeletonising the channel mask (Fisher et al., 2013; Pavelsky & Smith, 2008) and then subsequently vectorising the medial axis pixels from the upstream end to the downstream end, provided no multiple channel patterns such as anabranching occur in the channel mask, or, in a recently developed approach, by computing the shortest path between the planform endpoints (Schwenk et al., 2016).

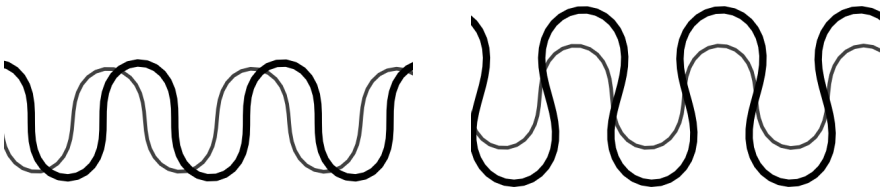

(a)

Figure 2: Illustrative examples of meander migration modes generated by a periodic mathematical model. (a) Purely downvalley migration. (b) Purely crossvalley migration.

The most common approach in studying the planform evolution of river meanders is to determine the migration rates and direction of their channel centerline. The average channel migration at the reach or subreach scale can be computed by the area between two channel centerlines obtained from temporally subsequent images divided by their average length (e.g. Constantine et al. 2014; Constantine 2006; Schwenk et al. 2016; Schwenk & Foufoula-Georgiou 2016). Conversely, local river bank erosion and accretion rates can be quantified by computing the minimum distance transform of two temporally subsequent river banks (Peixoto et al., 2009; Rowland et al., 2016; Schwenk et al., 2016). Lauer (2006) implemented a centerline-based method for calculating the rates of centerline migration in a GIS environment (ArcGIS Channel Planform Statistics toolbox), which is more inherently consistent with the approach used in meander morphodynamic models (Seminara et al., 2001). This tool interpolates a sequence of Bèzier curves between subsequent channel centerlines and cumulates their orthogonal distances. However, such a method fails close to the apexes of meander bends when the migration is dominantly downvalley (Figure 2a, see Aalto et al. 2008; Lauer & Parker 2008), while generally succeeding where the migration is predominantly crossvalley (Figure 2b).

1.3. The need for automated extraction of information on river meander morphodynamics

There are four main reasons that enhanced better automation in the extraction of meander morphodynamics information from multispectral remotely sensed data is required. First, to date there is no software, to our knowledge, that can perform a robust river centerline extraction from multispectral data and that is able to automatically detect the centerline of the main channel when the channel bifurcates into a main and a secondary channel. Robust extraction is further complicated by the presence of tributaries and abandoned channels which are involuntarily incorporated in river masks. On the other hand, difficulty in capturing the main flow is enforced by the presence of secondary channels and anabranching structures; in the following, we will assume that the main flow occurs in the widest channel. Second, river planform migration rates computed with existing methods necessitate manual correction as these methods are not able to determine the migration rates close to the bend apexes with an acceptable accuracy. Third, to our knowledge, the multitemporal analysis of instream sediment bar dynamics is still performed through manual procedures by means of GIS tools, thus limiting reproducibility. Finally, a systematic feedback between models and observation is still limited by the scarcity of comparable data: although a large quantity of remotely sensed data (e.g., Landsat, Sentinel, MODIS) is currently available, such data needs to be processed in a simple and efficient way to be suitable for systematic analysis and comparison with increasingly used river morphodynamic models.

The aim of this research is to develop and test a fully automated, process-based software (PyRIS) for the extraction of extensive meander morphodynamic information from multispectral remotely sensed images through three main steps:

(i) river planform centerline extraction, (ii) computation of local centerline migration rates and (iii) multitemporal analysis of sediment bar dynamics; PyRIS provides a significant improvement on the state of the art by implementing such computations in a fully automated and process-based manner.

1.4. Comparison of PyRIS *to currently available software*

PyRIS is a process-based software, in the sense that its implementation is strongly based on process-based analytical models that have been developed in the last decades. Similarly to the aforementioned Rivmap, PyRIS is specifically designed for the morphodynamic analysis of single- and multi-thread meandering rivers, but with a different goal: PyRIS aims at providing an easy-to-use tool for extensive multitemporal analysis of large datasets. Its utility mainly comes from its portability and scalability on different river contexts, and secondarily on the preciseness of the algorithm.

An extensive comparison of morphodynamic analysis engines including a set of nine software tools can be viewed in Rowland et al. (2016). Schwenk et al. (2016) compared the recent software Rivmap against the most relevant ones in the context of river morphodynamics among those cited by Rowland et al. (2016). Here we provide a brief overview of the differences between PyRIS and a selection of some of the most recently developed software that are relevant to our context. Most of the currently available software are written in proprietary programming languages such as MATLAB (Rivmap by Schwenk et al. 2016 and ChanGeom by Fisher et al. 2013) or IDL (RivWidth by Pavelsky & Smith 2008 or SCREAM by Rowland et al. 2016) that make them unavailable except upon license. PyRIS is open source as it is written in the Python language and is freely available (see section 8.1).

PyRIS computes the channel masks directly from remotely sensed data, while currently available programs require the channel mask to be computed externally by the user; moreover, PyRIS is able to include bare sediment such as emerging bars in the channel masks. Rivamap by Isikdogan et al. (2017) can compute channel masks from multispectral images but based on a single spectral index that contrasts between and water and land (they use the MNDWI – Modified Normalized Difference Water Index). The migration rates computed by PyRIS are centerline-based and its algorithm is currently the only one allowing to detect both the magnitude and the direction of migration of each centerline point. Finally, PyRIS is the only morphodynamic analysis engine able to detect and analyse river bars.

2. Data

PyRIS is specifically designed for the Landsat Level1 Product (`http://landsat.usgs.gov/`), from which it can extract river masks by combining the spectral bands. However, PyRIS can also perform computations on river masks computed externally, hence skipping the mask extraction procedure. An example is provided in section 3.3, where the channel planform is extracted from digitized historical maps (see Figure 6).

Landsat Level1 Data Products consist of a wealth of multispectral data, with band designations including Visible (RGB), Thermal Infrared (TIR), Near and Middle InfraRed (NIR, MIR), Short Wave InfraRed (SWIR) and more. Analysis of Landsat archive has been successfully applied in the fluvial context by many authors, e.g. Constantine et al. (2014); Henshaw et al. (2013); Schwendel et al. (2015); Schwenk et al. (2016). Multitemporal analysis of Landsat data usually requires the application of an atmospheric correction to the image frames in order

to account for differences in cloud cover and exposition between image frames, when shared training data are applied for river detection. PyRIS, however, does not require any atmospheric correction since there is no classification where training data computed for a particular time frame is applied on other time frames (Song et al., 2001): the river planform is detected in each image frame individually and independently on the other time frames, hence, athmospheric correction is not necessary.

There are four Landsat types of data, namely

1. Landsat1–5 MultiSpectral Scanner (MSS): four bands, 60m resolution, 1972–1992;
2. Landsat4–5 Thematic Mapper (TM): 7 bands, 30m resolution, 1982–2012;
3. Landsat7 Enhanced TM (ETM+): 8 bands, 30m resolution, 1999–to date[1];
4. Landsat8 Operational Land Imager (OLI) and Thermal Infrared Sensor (TIRS): 11 bands, 30m resolution, 2013–today.

PyRIS requires Landsat Data belonging to the set of Landsat4–5 TM, Landsat7 ETM+ and Landsat8 OLI and Landsat8 TIRS for the computation of the river masks. PyRIS exploits the fact that some spectral bands have peaks in the absorption or reflection for particular types of landcover, such as vegetation (NIR), water (MIR) and minerals (SWIR).

The Landsat data must be preselected and downloaded by the user from the USGS's Earth Explorer website and placed into a single directory where PyRIS can iterate over each temporal scan in order to build the multitemporal analysis. The preselection should remove scenes where clouds are significantly covering the river body, scenes that are poorly georeferenced. Furthermore, from 2003,

[1]Data gaps since 2003

Landsat7 data is unfortunately corrupted by the presence of transverse no-data stripes over each band. Such products are marked as SLC-off. PyRIS provides an automatic workaround that consists in applying a greyscale closing operation to each of these bands. However, we recommend not to use the SLC-off products with PyRIS since the results would be strongly approximated in correspondence of no-data stripes. When the domain of interest spans on more Landsat scenes, PyRIS allows to automatically merge the scenes to cover the whole domain. Finally, the choice of Landsat as the standard input data poses an intrinsic limit to the spatial scale of rivers that can be processed through PyRIS: since the spatial resolution of Landsat bands on which PyRIS operates is 30m, the range of applicability consists of "large" rivers, for which an acceptable error could be achieved. For instance, in a 300m wide river (ten times pixel resolution) if two pixels (one per riverbank) are misclassified, this would yield a 20% error.

3. Methods

We illustrate the core methods and algorithms implemented in PyRIS. PyRIS is written in the Python language and makes convenient use of the object-oriented properties of such language. Several freely-available, non-standard Python libraries are required, namely NumPy (Oliphant, 2006), SciPy (Jones et al., 2001), Scikits-Image (Van der Walt et al., 2014) and GDAL (Butler, 2004).

The sequence of computations provided by PyRIS can be summarized as follows: (i) river mask extraction from raw multispectral data; (ii) planform extraction from the river mask; (iii) separation of individual meander bends and computation of the local centerline migration vectors; (iv) analysis of the sediment bedform dynamics.

3.1. River mask extraction

PyRIS extracts of the channel network by a pixel-based thresholding which combines the following image derived data layers/bands:

1. NDVI (Normalized Difference Vegetation Index);
2. MNDWI (Modified Normalized Difference Water Index);
3. SWIR (Short Wave InfraRed Band).

By combining indexes 1–3 PyRIS automatically delineates the river body by considering water and sediment, and it enforces river boundaries delineation by excluding vegetated pixels. Specifically, the exclusion of vegetated pixels from the river body is performed through an approach similar to that proposed by Subramaniam et al. (2011), relying on the NDVI (Carlson & Riziley, 1997), which assigns a brightness value to each pixel proportionally to its vegetation percentage. Water pixels are included by computing pixel values of the MNDWI index (Xu, 2006), which computes a brightness value depending on the percentage of water in the pixel (Xu, 2005; Subramaniam et al., 2011; Lu et al., 2011; Feyisa et al., 2014). On the other hand, natural rivers usually display a component of emerging sediments that belong to the morphologically active channel, and as such are submerged under bankfull conditions. For sediment bars to be included in the river body we employ the SWIRband (band 7 in OLI, TIRS and TM Landsat missions), as recommended by the USGS (`https://www2.usgs.gov/faq/node/3859`) in order to detect mineral deposits.

Each of the data layer undergoes a thresholding procedure in order to obtain three different masks. The thresholding is performed through the Otsu thresholding method (Otsu, 1979), which computes the brightness histogram of the classifier and defines a threshold value by assuming that two classes only exist

and by maximizing their interclass variance. The thresholding procedure is applied to the NDVI and MNDWI classifiers, while the SWIR band is normalized (floating point values between -1 and +1) and then thresholded to the value 0. Such a procedure on the SWIR band was necessary as the area covered by the emerging sediment is typically small, hence the histogram frequencies would eventually be too low for class recognition in the Otsu thresholding method. Once each of the classifiers as been thresholded, we obtain three binary masks, which consist of binary images denoting whether the classifier value is above or below the given threshold, hereafter identified by white and black respectively. Figure 3 illustrates the three classifiers associated with their specific masks.

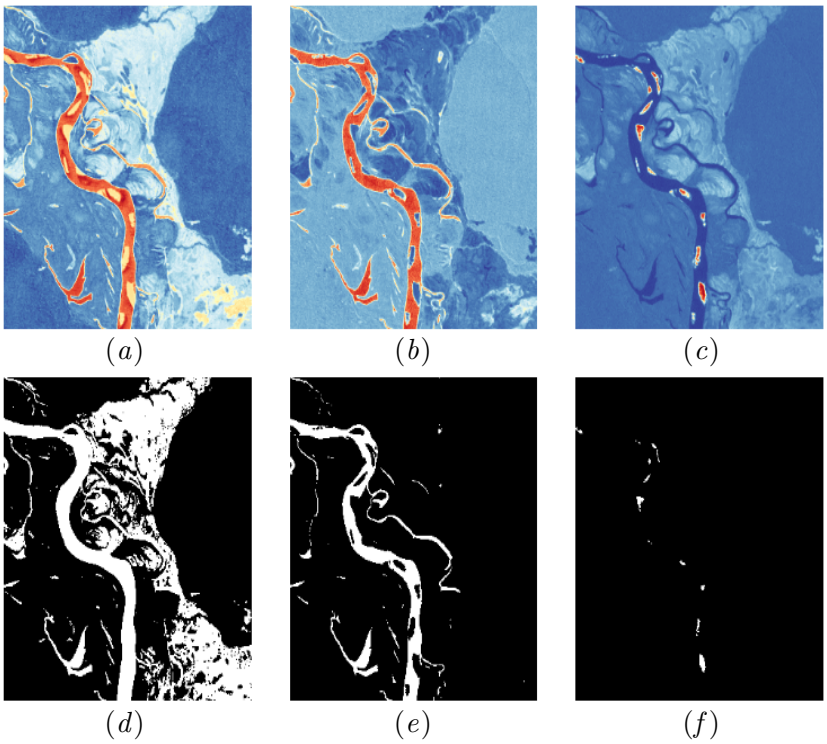

Figure 3: Application of 3 classifiers to a reach of the Xingu River (Brazil) and thresholding (the panels show a zoom of a larger mask). (a) NDVI index. (b) MNDWI index. (c) SWIR band. (d) Thresholding of the NDVI index. (e) Thresholding of the MNDWI index. (f) Thresholding of the SWIR band.

297 PyRIS computes the river mask by means of well established binary morpho-
298 logical operations involving the three masks, such as dilation, erosion, opening,
299 closing (Haralick et al., 1987; Serra, 1986, 1982). First, the MNDWI mask is
300 dilated through a structuring element scaled by a fraction of a user estimated
301 magnitude of the average river width. An intermediate mask is then created by
302 applying a `binary_and` operator (intersection set) to the NDVI and the dilated
303 MNDWI masks (i.e., the intermediate mask corresponds to the product of the
304 two masks). A `binary_or` operation (union set) between such intermediate mask
305 and the segmented SWIR mask allows us to account for emerging sediment bars

in the final mask (i.e., the sediment mask complements the intermediate one). Binary noise due to either tributaries, clouds, small water bodies such as oxbow lakes and humidity is removed through a binary filter combining `binary_opening` operations and iterative removal of small objects (Figure 4). Large water bodies and objects that do not belong to the river reach can be excluded by the user: upon the user request, PyRIS opens a window where the user manually draws areas that needs to be excluded from the analysis; this operation is done once for all the multitemporal dataset. Afterwards, the binary filter that we implemented in PyRIS allows to remove the remaining isolated objects left in the water mask, thus only maintaining the noise connected to the channel mask (Figure 4), which is removed by the pruning and axis extraction algorithms.

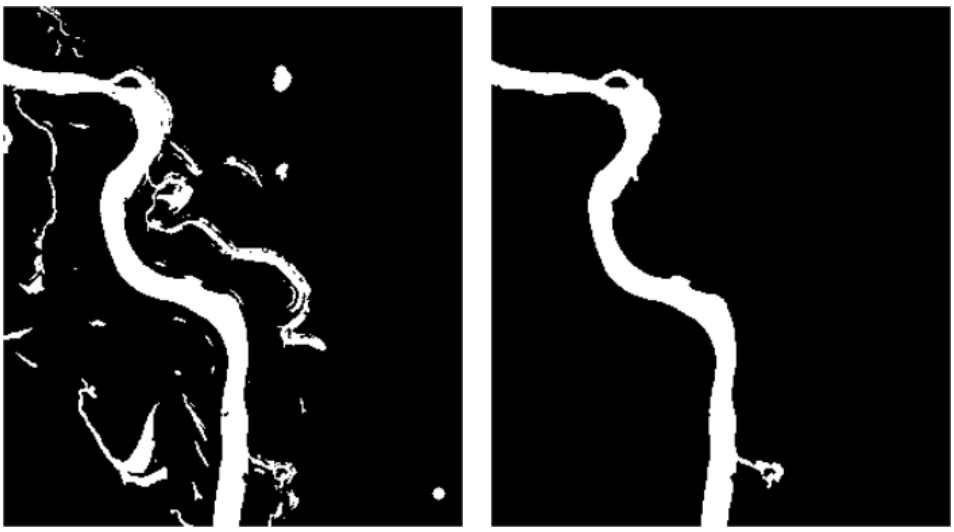

(a) (b)

Figure 4: Binary mask of the Xingu River as obtained by merging the three individual masks reported in figure 3 (zoom of a larger mask). (a) Before binary noise removal. (b) After binary noise removal.

3.2. Planform extraction: centerline coordinates, curvature and channel width

Common algorithms for the extraction of the channel centerline from a binary mask are specifically designed for a very trivial scenario, i.e. when the mask holds, from a mathematical point of view, a simply connected set of pixels (Fisher et al., 2013; Pavelsky & Smith, 2008; Rowland et al., 2016). A recently developed approach by Schwenk et al. (2016) enables the extraction of the centerline in the multibranching scenario by computing the shortest flow path. However, the shortest path does not generally represent the main flow path, since the latter may avulse over longer branches. As an example, chute channels are shorter than the main channel, but they usually carry a smaller amount of discharge; they can eventually grow in size after significant floods and become the main channel leading to chute cutoffs, but such a complex process cannot be captured by a planform extractor that selects the shortest path. The centerline extraction typically proceeds through a skeletonisation algorithm (e.g. Zhang & Suen 1984) followed by a pruning of the skeleton (e.g. Bai et al. 2007; Choi et al. 2003) which allows to remove spur noise. Hence, when a mask contains holes denoting either a bifurcation, a chute channel or an anabranching structure, one would be interested in extracting the path of the main channel, i.e. the path with the larger average channel width. With an algorithm specifically designed for this latter scenario one would also automatically be able to filter out residual branches whereby binary noise due to tributaries and oxbows occurs.

In PyRIS we applied a skeletonization procedure followed by a pruning algorithm. Skeletonization is applied simultaneously with the computation of the distance transform of the river mask, whereby each pixel of the channel mask is given the value of its distance from the nearest non-river pixel. The channel width is approximated as twice the value of the distance transform computed

along the channel centerline. Such a pruning algorithm allows for removing the remaining spur noise connected to the channel skeleton (Figure 5). Some of the noise may eventually remain and it will definitely be cleaned later by the centerline vectorisation, which will run over the noisy branches and properly mark them as noise. Therefore, the only aim of the pruning algorithm here is to reduce the computational effort of the centerline vectorisation.

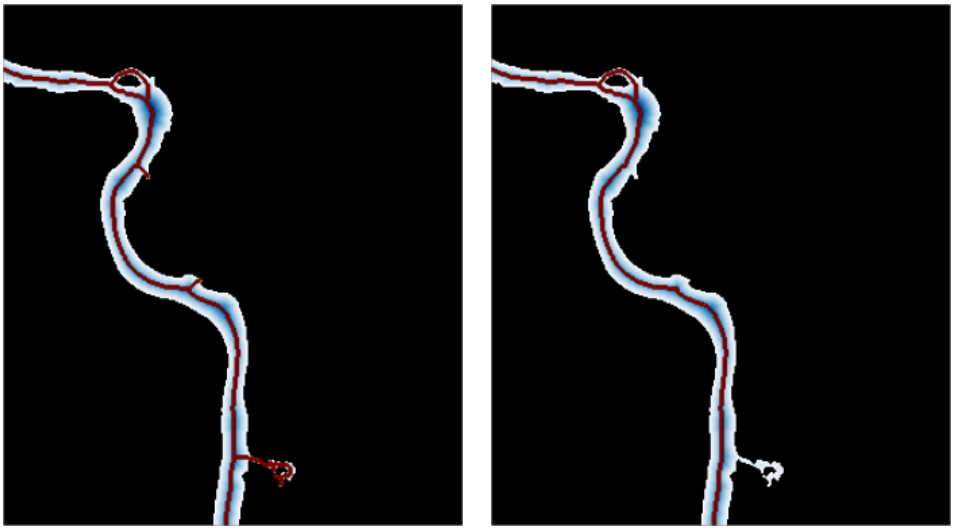

(a) (b)

Figure 5: Distance transform (white-to-blue colormap) and skeletonization (red line) on the Xingu River mask presented in Figure 4b (zoom of a larger mask); (*a*) Before pruning, with spur noise (50 iterations). (*b*) After pruning, spur noise removed (50 iterations).

In order to extract the centerline, the skeleton of the river mask must be vectorized. In other words, its points must be read as coordinate pairs (x, y) in *upstream-to-downstream* order. Vectorizing the centerline is a trivial operation when the skeleton consists of a unique branch, i.e. it does not bifurcate and spurs are removed, (e.g. Dey & Bhattacharya 2013; Fisher et al. 2013; Pavelsky & Smith 2008; Rowland et al. 2016). Such operation requires to read the centerline points *neighbor-after-neighbor* starting from the inlet point straight down to the outlet.

A more sophisticated procedure must be adopted in the case in which bifurcations, chute and secondary channels or residual spurs are present. The latter is the case of many natural river systems, and especially of the world's largest rivers, which tend to develop anabranching patterns in their lowland courses, for which a correct and robust identification of main channel is required. In PyRIS we implemented a centerline vectorisation algorithm which is automatically able to distinguish the main channel from secondary ones by means of a recursive procedure which analyses all the possible paths the flow could take: at each bifurcation of the centerline, the PyRIS algorithm checks the downstream path of all the branches and selects objectively the one representing the main channel through the algorithm described below. It is important to note that this procedure also allows for removing automatically from the planform all the spur noise left from the pruning algorithms. In fact, in most software applications the pruning algorithm must be iteratively run from the user until convergence is reached because the number of iterations required is not known *a priori*.

The work-flow of the centerline vectorisation algorithm of PyRIS can be summarized as follows:

1. automatically locate initial point of the centerline;
2. save current point into a coordinate list;
3. move to neighboring point and remove current point from skeleton;
4. iterate steps (2)-(3) until either one of the following conditions is matched:
    (a) no neighbors are found;
    (b) more than one neighbor are found;
5. if (4a) is matched, then the end of the branch is found and returned;
6. if (4b), then start from each of the neighboring points and run recursively through steps (2-7)

7. append to the coordinate list the main channel branch through a selection procedure.

Every time a bifurcation is encountered, the main channel path is selected by analyzing the downstream branches: of such branches, the average widest path in terms of channel width is selected, except in some specific cases (when a branch connected to the whole downstream reach is shorter than 75% of the other one connected to the whole downstream reach, it is discarded, because it would represent either a cutoff residual or a spur branch). PyRIS implements other possibilities for the definition of the main channel, namely the selection of the widest/narrowest branch and of the longest/shortest one.

Once the centerline coordinates are vectorized, i.e. two arrays containing x and y values in terms of pixel positions are computed, they are georeferenced through the geographical transform metadata included in the remotely sensed data when available. The geographical reference allows for representation of the centerline properties in proper geographical coordinates and superposition of multiple planform shapes from different time periods. Once the centerline points are computed, a Parametric Cubic Spline (PCS) interpolation is performed (Güneralp & Rhoads, 2007), where a smoothing factor is eventually applied in order to avoid aliasing effects and the resulting high frequency noise when computing the channel curvature. The value of the smoothing factor is the midpoint of the range suggested by the Python library.

Centerline arc-length s_i, inflection angle $\theta_i(s_i)$ and curvature $\mathcal{C}_i(s_i)$ for each

coordinate pair (x_i, y_i) are readily computed, respectively, as

$$s_i = \sqrt{(x_i - x_{i-1})^2 + (y_i - y_{i-1})^2}, \tag{1a}$$

$$\theta_i = \arctan\left(\frac{y_i - y_{i-1}}{x_i - x_{i-1}}\right), \tag{1b}$$

$$\mathcal{C}_i = \frac{\theta_{i+1} - \theta_{i-1}}{s_{i+1} - s_{i-1}} \tag{1c}$$

together with local values of channel width. The latter is approximated by the values of the distance transform of the river mask computed at the centerline points.

3.3. Local migration vectors and individual bend separation

We implemented a centerline migration algorithm that is able to compute the local vectors (magnitudes and directions) of the migration of the river planform centerline. The zero crossings of the centerline curvature spatial distribution are denoted as *inflection points* separating individual meander bends, which are in turn labeled and linked throughout the temporal evolution of the river centerline (see Figure 6).

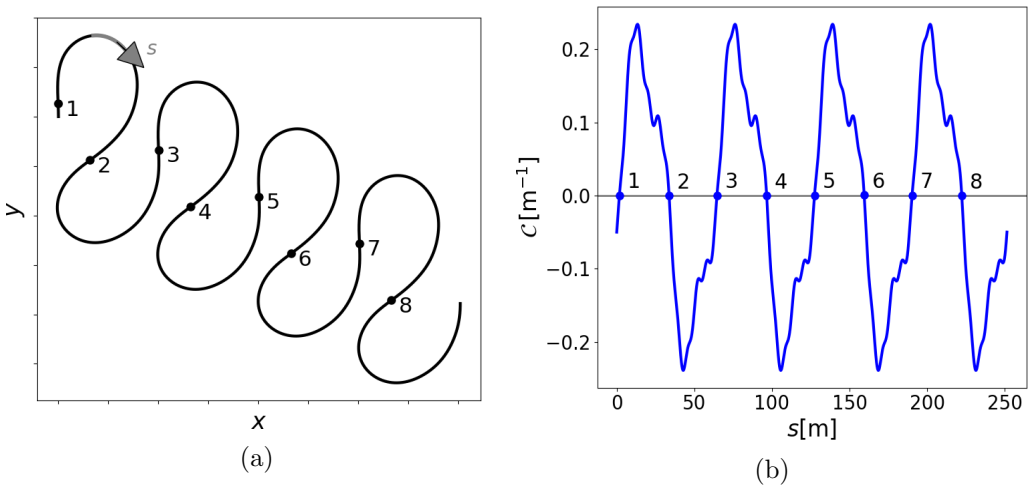

Figure 6: Sketch for bend separation in PyRIS. (a) Synthetic planform centerline. (b) Curvature distribution along the centerline. The s coordinate denotes the downstream coordinate of the channel axis (equation 1a), $\mathcal{C}$ is the local intrinsic curvature of the centerline (equation 1c). The dots correspond to the inflection points (zero-crossings of the centerline curvature distribution) separating individual meander bends. The numbers represent the indexes of the corresponding meander bend (downstream with respect to the inflections).

If the user does not require the application of the smoothing procedure to the channel centerline during the planform extraction (see previous section), PyRIS enables for the filtering of the high frequency noise of the intrinsic curvature distribution of the planform centerline by computing a smoothed PCS. This is particularly relevant for bend separation because high-frequency noise creates a large number of nonphysical inflection points on the channel axis. The inverse transform allows the exclusion of the high frequency noise from the channel curvature by comparing its scales of oscillations with those of the dominant frequencies in the curvature signal, which are orders of magnitude longer. Once the curvature is filtered, the remaining inflection points can be isolated and correlated through time when performing multi-temporal analysis as proposed by Schwenk & Foufoula-Georgiou (2016).

We computed the local migration vectors following a *bend scale* approach.

For each individual meander bend of the planform at some time frame, a PCS interpolation is made for the configuration of the same bend in the next time frame, in order to have a biunivocal point-to-point correlation, i.e. the centerlines are resampled to have the same number of points. Then each centerline point migrates into the correspondent point (having the same rank) in the bend centerline at the next time frame. Migration vectors are determined as the spatial segments connecting each pair of correlated points. Finally, we set thresholds on the temporal variation of individual bend metrics (sinuosity and length) in order to capture bend cutoffs, for which the migration vectors are not computed. Bend length is defined as the portion of centerline arc-length between two inflections; bend sinuosity is the bend length divided by the Cartesian length between the two inflections; when a bend undergoes cutoff, i.e. it cuts itself out, its sinuosity and length drop significantly and it does not make sense to compute the migration vectors.

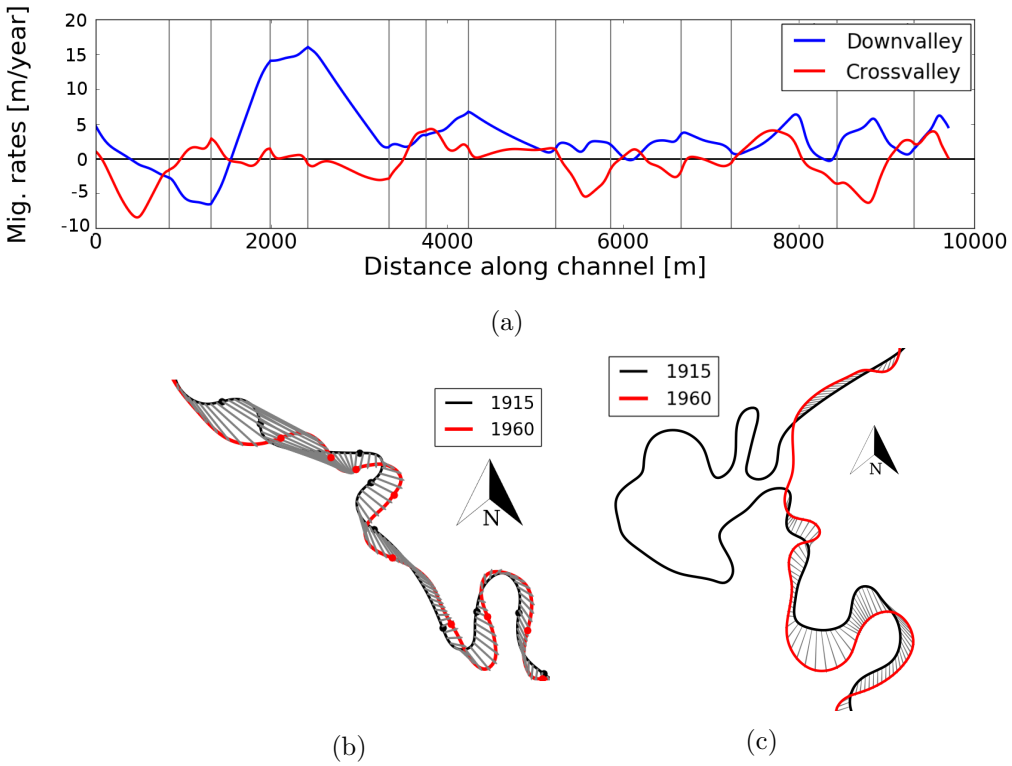

Figure 7: Local migration rates for a reach of the meandering Prut River (border between Romania and Moldova, Bisht et al. in progress) between 1915 and 1960. Centerlines have been extracted by river masks digitized from historical maps with 1m resolution (Bisht et al., in progress). (*a*) Local migration rates of the centerline reported in figure (*b*) reprojected in the local downvalley and crossvalley direction. Vertical lines indicate inflection points. (*b*) Migration vectors plotted as arrows (gray) between the two planforms. Thick dots on the planform centerlines represent the inflection points. (*c*) Identification of a large cutoff on another reach of the Prut River. PyRIS automatically recognized that no migration rates have to be computed for the bends that have been cut off.

The x and y components of the local centerline migration vectors can be reprojected on different directions, such as downvalley and crossvalley (Figure 7). Note that the massive downward shift in the first few bends of the Prut River (Figure 7b) is correctly represented by the downvalley migration blue curve in Figure 7a, whereas nearly no crossvalley migration is observed (red line). Local downvalley and crossvalley directions are defined for each individual bend. The

local downvalley direction is defined as the direction corresponding of the straight line joining the inflection points of the bend, while the local crossvalley direction is the one orthogonal to the downvalley one and points towards the bend apex.

3.4. Sediment bar dynamics

A specific feature of PyRIS compared to existing software is an automated procedure that allows for systematic and quantitative analysis of the dynamics of sediment bars in meandering, single-thread rivers by using multispectral remotely sensed data. PyRIS extracts properties of bare sediment surfaces viewed as bars regardless of their morphodynamics properties. The extracted properties allow the user to distinguish between sediment bars that migrate along the channel and the point bars, which tend to remain fixed with respect to the channel planform.

The analysis of longitudinal and lateral movement of steady and migrating channel bars in evolving meander bends is conveniently performed with reference to a dimensionless, intrinsic coordinate reference system (s,n). The (s,n) system of coordinates (Merwade et al., 2005; Legleiter & Kyriakidis, 2006; Luchi et al., 2011; Smith & Mclean, 1984) is locally aligned with the curvilinear arc-length of the channel centerline, normalized by the averaged channel half-width (s) and the direction orthogonal to the channel axis, normalized by the local channel half-width (n), respectively. The coordinate s ranges from 0 (first point of the planform) to the length of the examined reach, divided by the average channel half-width. Coordinate n ranges between -1 for the right bank and $+1$ for the left bank; $n = 0$ represents the transverse position of the channel centerline.

The coordinate transformation from a Cartesian (x, y) system to the orthogonal curvilinear (s, n) system results into a straightened equiwidth representation of a meandering channel, on which we reproject the SWIR band values. PyRIS

then identifies the sediment bars at each time frame through a thresholding procedure (analogous to the one performed to compute the sediment mask described earlier) on the reprojected SWIR data of the image. This procedure automatically identifies the regions occupied by individual bare sediment bars in each image frame. Each bar is uniquely labeled by assigning it a Bar Index, which is a unique integer number ranging from 1 (upstream) to the total number of bars (downstream), whereas the value 0 is assigned to channel regions in which no bare sediment appears. PyRIS computes the bar areas and bar centroids for each time frame.

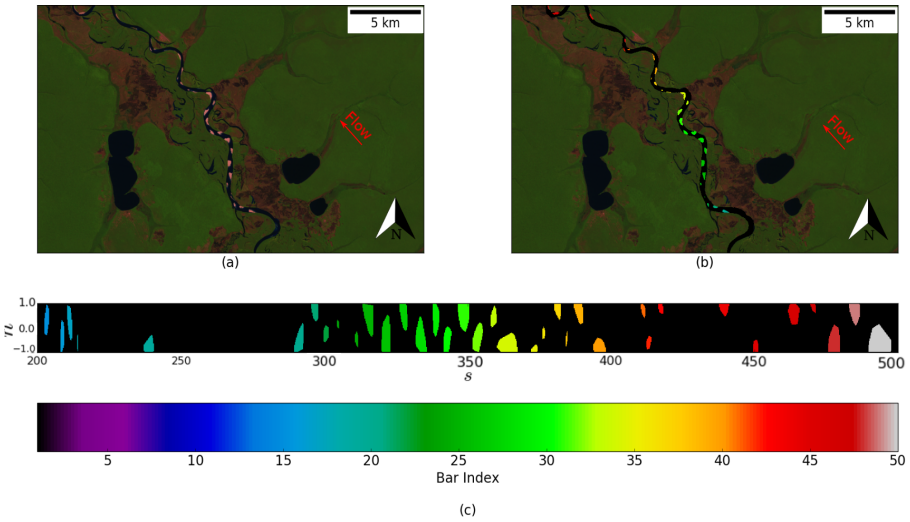

Figure 8: Automated bars detection, labeling and reprojection example from a reach of the Xingu River. (a) Landsat false color composite based on LT52250681984207CUB01_B(5,4,3).TIF image layers. (b) River mask and bar index over-imposed on the same false color composite. (c) River mask with labeled bars reprojected on the intrinsic reference system (above) and colorbar (below).

To analyze the temporal evolution of individual bars, each bar has to be tracked through different time frames. Such tracking is computed by a bend-scale selection based on thresholds on intrinsic and Cartesian distances. In other words, we identify sediment bars for each individual meander bend in a given time

frame and find its representation in the following time frame. The position of each bar is normalized by its position relative to the bend apex of an equivalent sine-generated curve, i.e. to the midpoint of the arc-length of the bend, and by the length of the entire bend, in order to filter out the effect of temporal bend elongation on the movement of the bar centroids (see figure 9). The bar migration rate of an individual bar is computed as the distance between the normalized positions of the centroids in subsequent time frames divided by the time window.

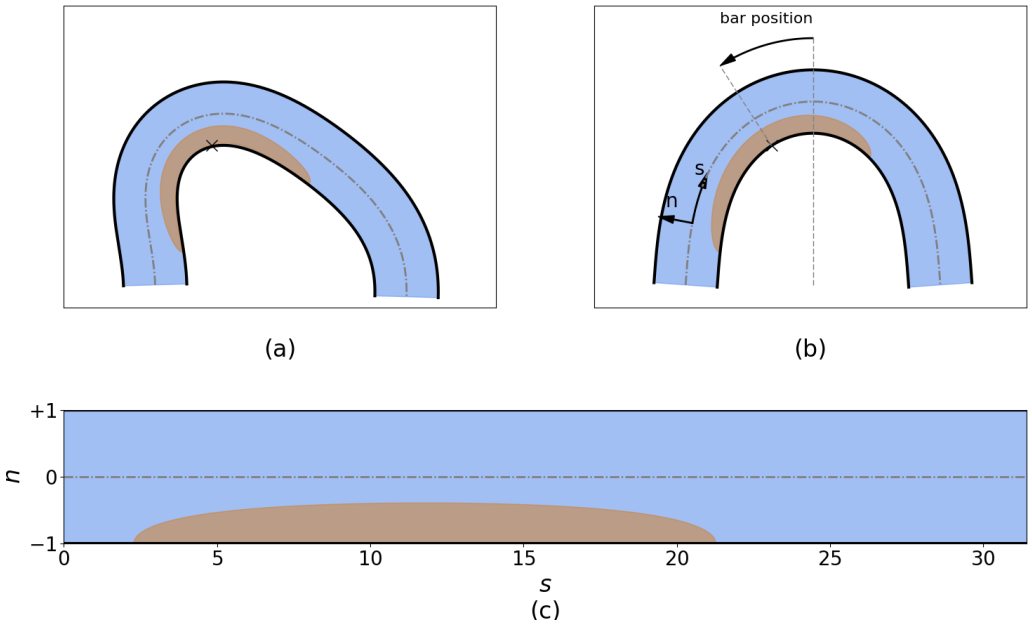

Figure 9: Sketch for the normalization of bar position in meander bends. (a) Original meander bend (the "x" marker represents the bar centroid). (b) Reprojection on the equivalent sine-generated meander bend. (c) Intrinsic (s,n) representation of the reprojection on the sine-generated meander bend.

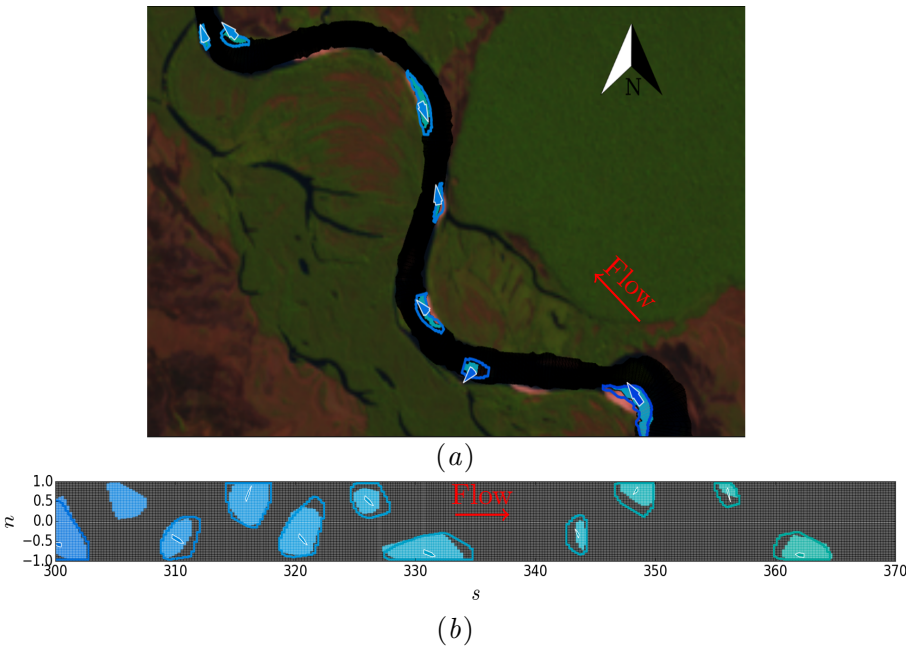

Figure 10: Correlation between river bars and their rates of downstream migration in PyRIS for the Xingu river. (a) Bar migration in georeferenced spatial coordinates (x, y). (b) Bar migration in the reprojected intrinsic reference system (s, n).

Each bar centroid is associated with an (x,y) coordinate pair and a corresponding (s,n) coordinate pair. PyRIS tracks each sediment bar within a river channel through time and computes the rates of its downstream migration v_c by differentiating in time the s coordinate of their centroids, with respect to the time interval $\mathrm{d}t$ between subsequent images

$$v_c = \frac{\mathrm{d}s_c}{\mathrm{d}t}, \tag{2}$$

where the pedix c indicates that values are referred to bar centroids. In addition, the wavelength L of each bar is computed by computing the spatial difference between the s coordinates of two subsequent bar centroids along the same bank

from the same time frame

$$L = s_{ci+1} - s_{ci}, \tag{3}$$

where the sub-pedix i indicates the index of bars that are numbered from upstream to downstream.

Finally, the streamwise coordinate for each individual meander bend is rescaled into the normalized bend arclength $\tilde{s}$ spanning between $\tilde{s} = -1$ (upstream inflection point) and $\tilde{s} = 1$ (downstream inflection point). The position of the bar centroid is reprojected at different time frames on the normalized arc-length $\tilde{s}$. In such a case, the point $\tilde{s} = 0$ represents the bend apex of an equivalent sine-generated bend. Figure 11 represents the position of a point bar in an evolving meander bend in the two reference systems, during few years of planform development of the river.

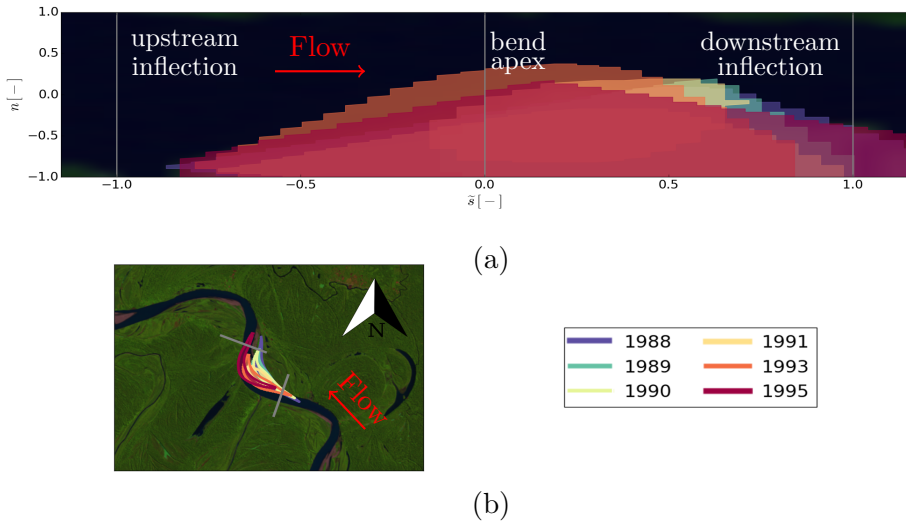

Figure 11: Temporal evolution of a point bar on an individual meander bend of the Ucayali River (Perù). (a) Point bar in the bend-scale normalized intrinsic reference system $(\tilde{s}, n)$. (b) Point bar on the geospatial reference system (x, y) superimposed on the Landsat real color composite based on LT05_L1TP_007065_20060901_20161119_01_T1_B(5,4,3).TIF image layers.

Figure 11b illustrates the position of the point bar in the geospatial reference

system, showing the intrinsic complexity of analysis of bar evolution when a meander bend is rapidly changing. On the contrary, in the intrinsic normalized reference system of panel 11a, the bar position with respect to the bend apex of an equivalent sine-generated bend highlights the evolutionary dynamics of the point bar independently from the temporal deformation of the meander bend.

4. Results: application of PyRIS

We illustrate several possible applications of PyRIS to show its potential in the investigation of the dynamics of the planform and large-scale bedforms (bars) of large meandering rivers in the Amazon basin. The focus of these applications is on the potential of the centerline extraction algorithm, on the sediment bar tracking method, and on the channel migration algorithm, which is tested against migration rates predicted by an analytical model of meander migration. We finally applied the migration algorithm to quantify the modes of migration of individual meander bends in a large meandering river undergoing a massive cutoff.

4.1. Planform extraction

PyRIS is able to automatically detect the main flow path in multi-thread reaches, like in the case of meandering rivers with chute channels and of anabranching systems. Figure 12 illustrates the results obtained by applying the sequence of algorithms presented in section 3.2 to morphological configurations in which abrupt diffluences from the main flow direction occur (the default main channel selection method is employed). Figure 12a shows the extraction of the main channel (red line) from large anabranching structures in the Amazon River. Figure 12b and 12c highlight the ability of PyRIS to capture chute cutoffs and abrupt main channel changes at bifurcations: in Figure 12b a bifurcation is evolving over

time and at some point the main channel switches from one branch to the other. Conversely, neck cutoffs (12c) are trivial to capture because only one channel is commonly active at each time provided the flow stage is not too high.

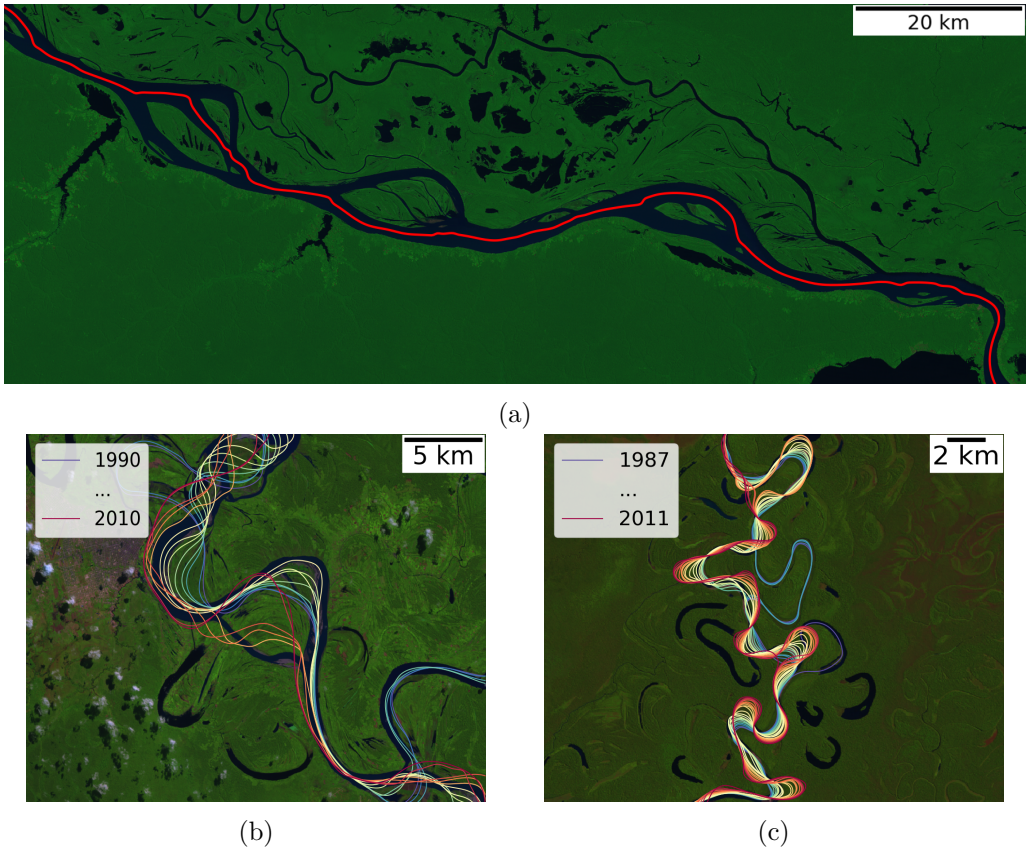

Figure 12: Multitemporal extraction of planform centerlines for an anabranching river, plotted over Landsat false color composites. (*a*) Main channel of a reach of the anabranching Amazon River (Brazil, Landsat false color composite based on LT50010622000042CUB00_B(7,4,2).TIF image layers). (*b*) Chute cutoff on the Ucayali River close to the city of Pucallpa (Peruvian Amazon, Landsat false color composite based on LT05_L1TP_007065_20050712_20161125_01_T1_B(5,4,3).TIF image layers). (*c*) Abrupt main channel change at a bifurcation and multiple neck cutoffs on the Rio Beni (Bolivia, Landsat false color composite based on LE70010692000178COA00_B(5,4,3).TIF image layers).

4.2. Individual bend separation and migration rates

We tested the methodology that we utilized in PyRIS for computing centerline migration rates against the migration rates obtained from an analytical

model for meander evolution (Zolezzi & Seminara, 2001; Seminara et al., 2001). For the testing, we used a synthetic periodic planform, which is commonly used in theoretical morphodynamic models for meandering rivers, because of its capacity of isolation and quantification of individual physical processes occurring during planform evolution of meander bends. The morphodynamic model we used assumes that every centerline point migrates outwards orthogonally to the local tangent of the centerline. Since the migration magnitude depends on the curvature distribution, each point has a different net migration rate, leading to a net non-orthogonal migration between large timesteps (the centerline is not resampled at each time step). Therefore, we calculate the migration of individual points of the centerline between the initial and the final configurations and compare them with the ones extracted through the PyRIS centerline migration algorithm (Figure 13a).

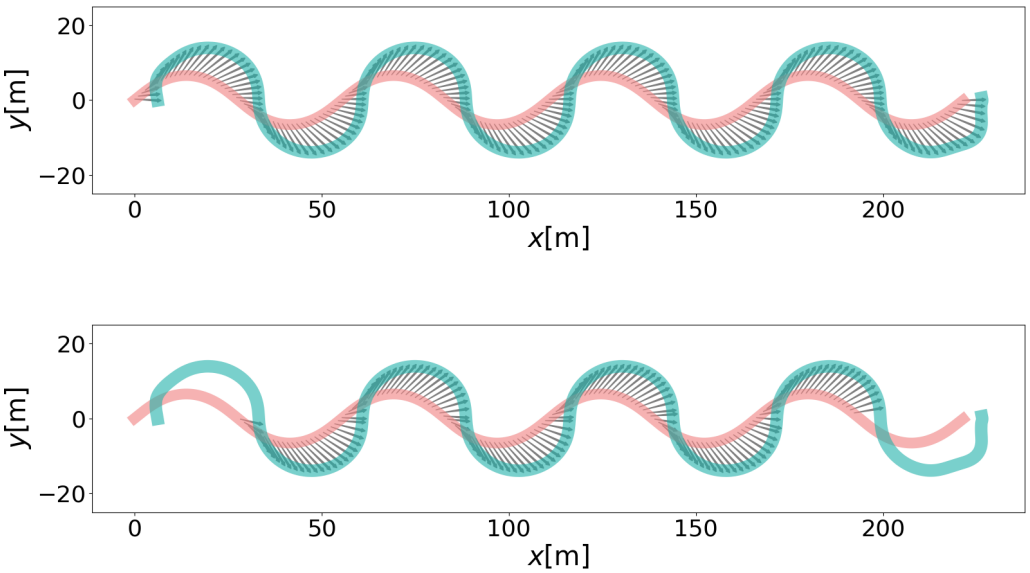

(a)

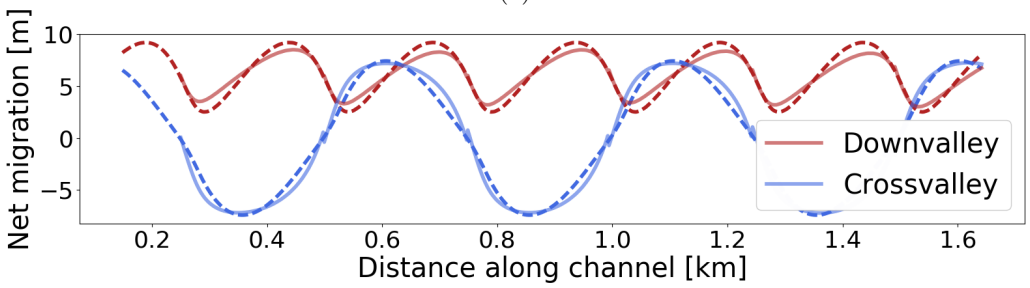

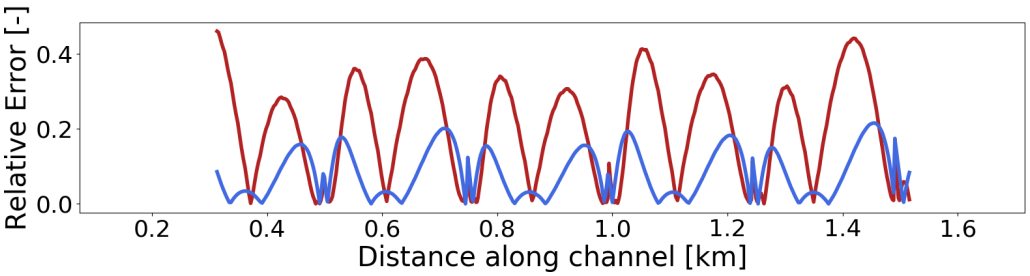

(b)

Figure 13: Validation of the proposed methodology for the local centerline migration rates against the morphodynamic model of Seminara et al. (2001). (*a*) Local migration vectors according to the model (above) and those computed by PyRIS (below). (*b*) Downvalley and crossvalley migration rates computed by PyRIS (continuous line) and by the morphodynamic model (dashed line); values (above) and relative errors (below).

Figure 13b illustrates that PyRIS tends to underestimate the crossvalley migration rates (blue line), which, in this case, coincide with the migration rates in the y direction of Figure 13a. The local relative error in the lower panel of Figure 13b is computed as the difference between the local migration rate computed by PyRIS and that predicted by the morphodynamic model, divided by half the range of values. The error tends to be reduced when moving close to the inflection points and the bend apex. Conversely, the downvalley migration rates (here coinciding with the migration rates in the x direction) tend to be partly overestimated. The normalized root mean square errors (NRMSE) between the model-predicted migration rates and those computed by PyRIS are 0.106 and 0.050 for the downvalley and the crossvalley migration rates, respectively.

Figure 14 illustrates the application of PyRIS to calculate the migration rates of the Ucayali River after a massive cutoff (Abizaid, 2010). Remarkably, PyRIS is able automatically exclude the city of Pucallpa during the segmentation process, without need for manual cleaning before the mask extraction (e.g. Schwenk et al. 2016). In Figure 14a the channel centerlines close to the cutoff location are reported for several years, while panel 14b shows the values of local crossvalley and downvalley migration rates averaged over every individual bend of the planform between 1998 and 1999.

The implications of such a large cutoff on channel migration were discussed by Schwenk & Foufoula-Georgiou (2015), Schwenk et al. (2016) and Schwenk & Foufoula-Georgiou (2016), who used the ratio between migration areas and centerline lengths to quantify migration rates. This allowed the observation of the cutoff affecting the reach-scale planform dynamics through waves of increasing migration rates propagating both upstream and downstream. By computing the local migration magnitudes and directions through PyRIS it is possible to enforce

and further expand such findings by separately quantifying the modes of migration (downvalley, crossvalley) of individual meander bends in the proximity of the cutoff. Figure 14 shows that the cutoff largely promotes downvalley migration, both upstream and downstream, over crossvalley migration; the magnitudes of downvalley migration upstream (smaller bend indexes) and downstream (larger bend indexes) of the cutoff are considerably larger compared to those of crossvalley migration for the same bends.

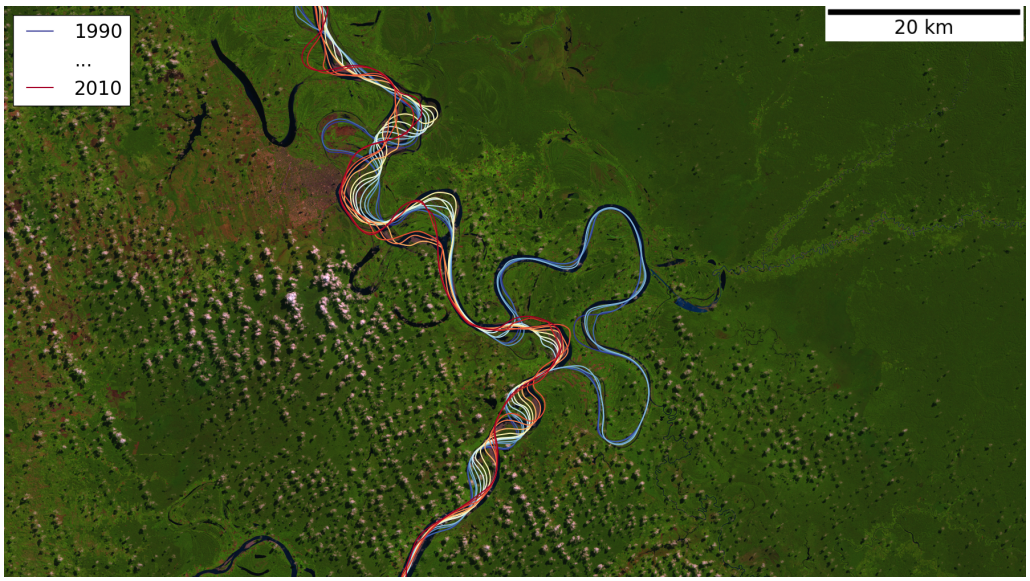

(a)

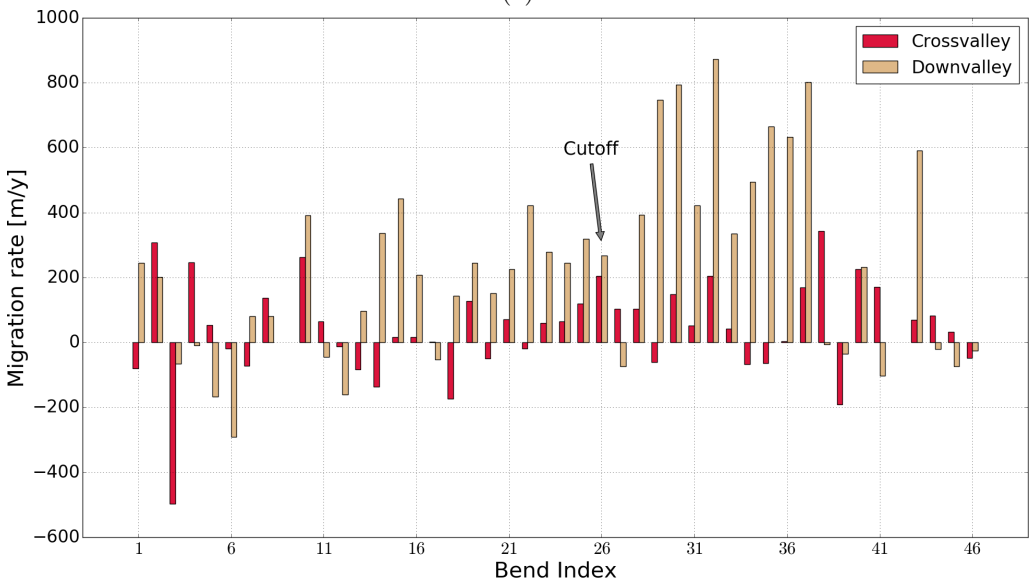

(b)

Figure 14: Assessment of downvalley and crossvalley migration rates after a massive cut-off on the Ucayali River (Perù) between 1998 and 1999. (*a*) Planform development highlighting the massive cutoff occurred in 1997 (Landsat false color composite based on LT05_L1TP_007065_20050712_20161125_01_T1_B(5,4,3).TIF image layers). (*b*) Bend-averaged local migration rates in the local downvalley and crossvalley directions.

4.3. Sediment bar dynamics

PyRIS is able to perform multitemporal analysis of sediment bar dynamics in single-thread rivers. An example of such feature is reported in Figure 15, which shows the spatial distribution of the local river bar migration rates in a reach of the Xingu River (Brazil) computed over 28 Landsat image frames between 1984 and 2011. The bar migration rates were initially computed as centroid-based discrete values, then they were interpolated over all the river pixels. The map shows the spatial distribution of local bar migration rates over more than twenty years, quantifying areas where the migration dynamics of bars within the channel are accelerated (red areas) or inhibited (yellow areas). The results here show that sediment bars along the Xingu reach tend to decelerate close to bend apexes, while moving much faster in quasi-straight reaches: a rate of movement of 0 means that either no bars are observed during the time period or steady bars only are observed. In the latter case, steady bars take the place of migrating bars close to bend apexes where the curvature is higher. This finding is consistent with theoretical models (see e.g. Tubino & Seminara 1990).

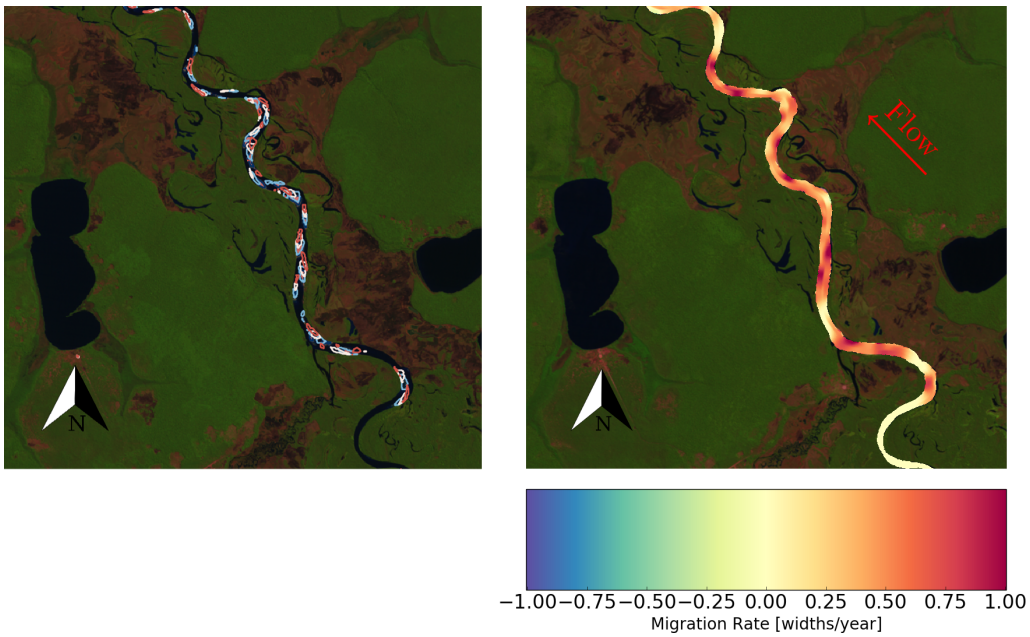

(a)

Figure 15: Spatially distributed local bar migration rates along a reach of the Xingu River (Brazil). The right panel shows the contour lines of bare sediment bars in years 1984, 1987, 1990, 1993 with colors ranging from blue to red as extracted by PyRIS. The left panel shows the spatially interpolated, temporally averaged rate of migration of bars along the channel in average channel width per year between 1984 and 2011 with colorbar.

5. Discussion

This work introduces PyRIS, a fully automated, process-based extractor of river morphodynamics from remotely sensed multispectral images. Though initially designed for multitemporal analysis of river meander morphodynamics, PyRIS also includes properties that can be useful for broader applications in the analysis of other river channel patterns, such as anabranching channels. In this section we discuss the main strengths, limitations and novel features of PyRIS in relation to its three main components (planform extraction, bend-scale analysis and local migration, sediment bar dynamics) described in section 3. The key foreseen steps for future work are finally summarized.

614 *5.1. Planform extraction*

615 The mask extraction procedure has been applied to several meandering and
616 anabranching river planforms, and each of them allowed extensive subsequent
617 analysis of centerline development, migration rates and bar dynamics. The
618 present manuscript focuses on selected applications on the Xingu River and
619 reports extracted centerlines on the Ucayali, Beni, Xingu and Amazon rivers.
620 The PyRIS mask extraction algorithm represents the first step in trying to
621 fully automate the mask and planform extraction process, which is still per-
622 formed through time-consuming procedures, either manual or computer-aided
623 (e.g. Güneralp et al. 2013). Moreover, our approach enables for multitempo-
624 ral analysis without requiring for atmospheric correction of Landsat data (Song
625 et al., 2001).

626 The applicability of such a procedure is partially restricted by the surrounding
627 landcover. The mask extraction is based on vegetation, water and sediment
628 indexes, reflecting its initial design for natural meandering rivers. However, in
629 most cases PyRIS is able to compute river masks from agricultural and partially
630 urbanized areas as well; in such cases a cross-check on the results is recommended.
631 PyRIS also allows to compute the river masks externally and to extract the river
632 planforms starting from river masks. It must be noted that, by accepting river
633 masks as input, PyRIS can potentially be applied to any kind of multitemporal
634 spatial data, including aerial and UAV-captured data.

635 The results should be evaluated by the user because the segmentation proce-
636 dure can be prone to errors, as pixels at river boundaries may be misclassified
637 if they contain a mixture of water, vegetation and sediment. Errors in the river
638 mask segmentation obviously affect the calculation of centerline migration and
639 sediment bar dynamics. Apart from geolocation errors and cloud coverage, a mas-

sive presence of urban areas around river bodies could lead to errors in classification. To partially cope with such issue, PyRIS allows the removal of potentially misclassified areas such as cities or water bodies before the run through a brief user interaction (areas are selected interactively). However, in our experience PyRIS is able to correctly extract river planforms in potentially urbanized areas: in the application to the Ucayali River (Figures 12 and 14), PyRIS was able to automatically classify the city of Pucallpa closely located to the river channel in a proper manner.

One important innovative feature of PyRIS is the recursive centerline extraction method, which builds the correct main channel path even in the case of complex morphological patterns. Related existing software (e.g. Fisher et al. 2013; Merwade 2007; Pavelsky & Smith 2008; Rowland et al. 2016; Schwenk & Foufoula-Georgiou 2015) instead require the main channel branch to be a-priori defined by the user. A similar approach, able to deal with multiple branches, was recently developed by Schwenk et al. (2016), but it can only account for the length of the branches and not for their width, leading to the extraction of the shortest path, which does not necessarily coincide with the main channel path: in fact, complex processes such as chutes and avulsions are very common in natural meandering rivers and most of the times the secondary channel is shorter than the main channel and carries a limited amount of discharge until it gets flooded and eventually becomes the main channel. By assuming that the largest branch coincides with the main channel PyRIS implements an improved treatment of multibranching channels compared to existing softwares. Although the widest channel may not represent the main channel in every single case (e.g., the widest channel could be a cutoff residual still connected to the river), most of the times this assumption holds true. To overcome such potential issue, PyRIS

cross-checks that the length of the selected main branch is not shorter than 75% of the second one. The selection of the widest path is based on the average values of the distance transform on the branches, which is known to fail on short reaches due to boundary effects; however, the distance transform here is computed on the whole mask, hence no boundary effects occur; in fact, based on our experience, the average widest branch is correctly selected for all the case studies.

Finally, the specific way PyRIS extracts multitemporal river planforms enables for capturing in an automated fashion discontinuous deviations from a main channel, i.e. when bifurcations, chute channels and cutoffs or anabranches occur, an operation that could not be perfomed automatically by existing related software.

5.2. Individual bend separation and local migration vectors

The PyRIS approach for computing the local channel migration vectors (magnitude and direction) enables to investigate meander morphodynamics with unprecedented level of detail and ensuring a high level of comparability between remotely sensed observations and river meandering morphodynamic models. The migration algorithm involves the separation and correlation of individual meander bends during time, allowing a straightforward comparison with the outcomes of river morphodynamic theories and models, which often reproduce the temporal development of individual meander bends taken as average representatives within a larger reach. The core advantage is the ability to correctly process migration rates in meander bends with dominantly downvalley mode of migration, overcoming previous limitations found in existing algorithms, which cannot correctly compute migration rates close to the bend apexes (e.g. Aalto et al. 2008; Lauer & Parker 2008). Moreover, whereas other existing software applications with simi-

lar goals can compute either an average value for a river reach (e.g. Constantine et al. 2014; Constantine 2006) or a local magnitude (Peixoto et al., 2009; Rowland et al., 2016; Schwenk et al., 2016) PyRIS provides a continuous representation of the migration vectors on the entire channel centerline. By reprojecting the migration vectors over the downvalley and crossvalley directions, PyRIS allows definition of the styles of migration of individual meander bends and of entire river reaches (PyRIS does not provide a definition for those, but they could be readily developed based on the PyRIS's framework). We illustrated one application of such reprojection together with the individual bend separation by defining the bend-scale styles of migration in the large meandering Ucayali River following a well-known massive cutoff (Abizaid, 2010; Schwenk et al., 2016; Schwenk & Foufoula-Georgiou, 2015). The robustness of the algorithm is supported by the quantification of deviations between the expected local centerline migration rates and those predicted by an analytical periodic model for meander planform evolution. Such deviations show an oscillating relative error which has a maximum NRMSE of $\mathcal{O}(10\%)$ for both downvalley and crossvalley migration rates of bend apexes and tends to vanish near meander inflections. Sources of errors on the calculation of migration rates are mostly related to the uncertainties in river mask extraction discussed in the previous subsection: in particular, geolocation errors may add a constant noise in terms of magnitude and direction.

5.3. Sediment bar dynamics

A completely novel feature of PyRIS is the methodology able to automatically investigate the dynamics of sediment bars along evolving meandering rivers, which potentially can be extended to a wider range of river channel patterns. Up to now, studies on the multitemporal dynamics of river bars have been limited

because of the constraints associated with the manual digitization of channel bars (e.g. Adami et al. 2016; Latrubesse et al. 2009). PyRIS allows to overcome such limitation and to automatically compute the spatial and temporal distributions of sediment bar migration rate, spatial occurrence and size. We applied the bar dynamics analysis for quantifying the distribution of large scale mobility of the channel bed along a river reach.

The requirements for the applicability of PyRIS to the computation of bar dynamics are represented by the availability of multi-spectral images within a range of flow stages allowing sediment bars to emerge from the water surface by a sufficient amount (i.e. area larger than the pixel resolution). Such conditions depend on both the flow conditions during remote sensing data acquisition and the resolution of the sensor. Flow stage changes may also change the position of the bar centroid with respect to its planimetric shape: this should be take into account by PyRIS users since it may drive to a small but persistent noise in bar migrations rates. Moreover, whereas central bars may be vegetated and therefore treated as islands by PyRIS, bank-attached bars that are completely covered by vegetation are not included in the river mask.

Finally, the issues related to the mask extraction, especially those related to data geolocation errors, may introduce errors to the results in terms of bar migration; once again, it is fundamentally important to check the data before running the script.

5.4. Future work

Future developments of the PyRIS software will focus on extending its present compatibility with Landsat data to other sensors that can provide appropriate river planform data. The choice of Landsat as the main data source for the analy-

sis performed in this study is because of its long-term availability. Mutlitemporal analysis of rivers, such as planform changes and sediment bar dynamics, necessitate to capture these dynamics, which can take multiple years to decades. In this context, Landsat provides the necessary temporal extent. One of the main limitations posed by Landsat data is their low spatial resolution, restricting the range of applicability of PyRIS to large rivers. As finer sensors that allow an increase of spatial resolution started to become available in recent years, e.g. the Sentinel missions, 10m per pixel, a compatibility with such datasets is planned to be implemented in PyRIS in the near future, to increase the range of river sizes at which the PyRIS software can be meaningfully applied.

6. Conclusion

Meandering rivers are one of the most widely studied earth surface systems, although knowledge on their dynamics is still limited. The scientific community is still lacking automated software that is able to extensively extract morphodynamic features from multitemporal remotely sensed data. To address this issue we introduced the process-based software PyRIS (Python–RIvers from Satellite) and illustrated its ability of extracting extensive information on the morphodynamics of meandering rivers with unprecedented automation levels.

PyRIS provides three main computations: (i) channel centerline extraction from either multispectral remotely sensed data or binary masks through a recursive algorithm able to capture the main channel at the occurrence of channel bifurcations, secondary channel and anabranching, (ii) the computation of local channel centerline migration rates and directions through a bend-scale approach, which provides a significant improvement to the state of the art through the ability of computing such rates in an proper manner even when the migration

rates is dominantly downvalley, and (iii) analysis of sediment bars dynamics by quantifying the local rates of change of the channel bed in evolving meander bends.

Our methodology for the local migration rates of the channel centerline compares well with analytical model outcomes, and normalized root mean square errors between PyRIS and model are quantified in the order of 10%. To our knowledge, our software provides the first successful attempt to quantify local sediment bar dynamics in evolving meandering rivers. We reckon that PyRIS can provide a significant improvement to the state of the art understanding of meander river morphodynamics, which can benefit researchers in river morphodynamics by allowing them to extract extensive information from multispectral remotely sensed data in a simple and fully-automated manner. Also in view of its potential of being applied to any kind of multitemporal spatial data (including aerial and UAV-captured data), PyRIS may have broader potential in river monitoring and management purposes, as for monitoring river discharge (Bjerklie et al., 2003) and as part of approaches for estimating sediment budgets from detected changes in river morphology (Fuller et al., 2003). Finally, though PyRIS has been specifically designed for the analysis of meandering or anabranching river patterns and morphodynamics, some of its algorithms (such as the one for the main channel detection) have the potential for broader applications, possibly including hemodynamics and remote navigation.

7. Acknowledgements

This work has been (partially) carried out within the SMART Joint Doctorate (Science for MAnagement of Rivers and their Tidal systems) funded with the support of the Erasmus Mundus programme of the European Union. The authors

are are grateful to Angus Morrison-Saunders, Blal Adem Esmail and Meili Feng for their helpful revisions and suggestions of the manuscript, to Tarun Bisht for his feedbacks on the testing the software.

8. Software availability and use

8.1. Availability

PyRIS is freely available for download on GitHub[2]. PyRIS is written in the Python language and requires the following free and open source libraries:

1. NumPy (`http://www.numpy.org/`);
2. SciPy (`https://www.scipy.org/`);
3. MatPlotLib (`https://matplotlib.org/`);
4. GDAL (`https://pypi.python.org/pypi/GDAL`);
5. Scikits-Image (`http://scikit-image.org/`).

The PyRIS source code is less than 1MB in size. It runs on any Linux distribution (freely available on the internet). However, Ubuntu is recommended. Windows and Mac users may consider the use of a virtual machine (VirtualBox–`https://www.virtualbox.org/`–is recommended and it is free). Landsat data is freely available on the website `http://landsat.usgs.gov/`.

8.2. User interface

PyRIS is both a command line script and a toolbox (a collection of functions that can be used in scripting for Python users). The use of the script is trivial also for users that are not familiar with the command line. On both Linux and Windows distributions it can be installed as a standard Python package (setup file

[2] `https://github.com/fmonegaglia/pyris`

is provided). For Windows users the Anaconda command line is recommended, which comes with a Python-Anaconda installations (`https://anaconda.org/`).

The script is run by simply calling the command `pyris` from the command line followed by arguments and options. The command `pyris <configfile> --init` creates a configuration file for the set of semotely sensed data concerning a single case study, which can be filled up by the user with few simple information (input/output paths, an order of magnitude of the channel width, the inflow direction). The configuration file can be edited for more fine tuning, such as number of maximum iterations for pruning algorithms and main channel selection criterion at bifurcations presented in the next sections.

Then, with the command `pyris <configfile> --select-black-mask <path to data>` the user can manually draw areas to be ignored during the analysis, such as large water bodies (sea, lakes, rivers). This is not mandatory except when other large water bodies appear in the domin and is done only once for an entire multitemporal analysis, taking only one or two minutes of trivial manual work.

The script can finally be run in fully automated mode with the command `pyris <configfile> -S -K -A -M -B --label auto`, where `S` is for Segmentation, `K` is for sKeletonization, `A` is for Axis extraction, `M` is for Migration rates and `B` is for Bars. Each option provides and operation that takes as input the output of the option of its left; for instance, if one is interested only in extracting the centerlines, she/he must also compute mask and skeleton but can leave out migration and bars (`pyris <configfile> -S -K -A`). At the end of this command the whole set of information is stored in the output path in a number of text files: river masks, river skeleton and tables containing sorted centerline coordinates, metrics, migration rates, bend indexes and bar positions and rates of change. Finally, the command `pyris --help` provides a brief manual of all

options and arguments that can be set when running PyRIS.

PyRIS took 4:31 hours to extract planform metrics and migration vectors of a 240km reach of the Xingu River from 28 individual Landsat 5 and 7 scenes on an Intel(R) Xeon(R) running a 3.20GHz CPU.

References

Aalto, R., Lauer, J. W., & Dietrich, W. E. (2008). Spatial and temporal dynamics of sediment accumulation and exchange along strickland river floodplains (papua new guinea) over decadal-to-centennial timescales. *Journal of Geophysical Research: Earth Surface*, *113*. URL: http://dx.doi.org/10.1029/2006JF000627. doi:10.1029/2006JF000627. F01S04.

Abizaid, C. (2010). An anthropogenic meander cutoff along the ucayali river, peruvian amazon. *Geographical Review*, *95*, 122–135. doi:10.1111/j.1931-0846.2005.tb00194.x.

Adami, L., Bertoldi, W., & Zolezzi, G. (2016). Multidecadal dynamics of alternate bars in the alpine rhine river. *Water Resources Research*, *52*, 8938–8955. URL: http://dx.doi.org/10.1002/2015WR018228. doi:10.1002/2015WR018228.

Amos, K. J., Croke, J. C., Hughes, A. O., Chapman, J., Takken, I., & Lymburner, L. (2008). A catchment-scale assessment of anabranching in the 143 000 km2 fitzroy river catchment, north-eastern australia. *Earth Surface Processes and Landforms*, *33*, 1222–1241. URL: http://dx.doi.org/10.1002/esp.1609. doi:10.1002/esp.1609.

Asahi, K., Shimizu, Y., Nelson, J., & Parker, G. (2013). Numerical simulation of river meandering with self-evolving banks. *Journal of Geophysical Research: Earth Surface*, *118*, 2208–2229. URL: http://doi.wiley.com/10.1002/jgrf.20150. doi:10.1002/jgrf.20150.

Bai, X., Latecki, L. J., & Liu, W. (2007). Skeleton pruning by contour partitioning with discrete curve evolution. *IEEE transactions on pattern analysis and machine intelligence*, *29*, 449–462.

van den Berg, J. H. (1995). Prediction of alluvial channel pattern of perennial rivers. *Geomorphology*, *12*, 259–279. doi:10.1016/0169-555X(95)00014-V.

Bisht, T., Monegaglia, F., Gramada, S., Zolezzi, G., & Pusch, M. T. (in progress). Morphometrics and morphodynamics of tight meander bends in a lowland european meandering river over one century, .

Bjerklie, D. M., Dingman, S. L., Vorosmarty, C. J., Bolster, C. H., , & Congalton, R. G. (2003). Evaluating the potential for measuring river discharge from space. *Journal of Hydrology*, *1–4*, 17–38.

Blondeaux, P., & Seminara, G. (1985). A unified bar-bend theory of river meanders. *Journal of Fluid Mechanics*, *157*, 449–470. doi:10.1017/S0022112085002440.

Brewer, P., Maas, G., & Macklin, M. (2000). A fifty-year history of exposed riverine sediment dynamics on welsh rivers. *BHS Occasional Paper*, *11*, 245–252.

Brewer, P. A., & Lewin, J. (1998). Planform cyclicity in an unstable reach: Complex fluvial response to environmental change. *Earth Surface Processes and Landforms*, *23*, 989–1008. doi:10.1002/(SICI)1096-9837(1998110)23:11<989::AID-ESP917>3.0.CO;2-4.

Butler, H. (2004). A guide to the python universe for esri users. In *Annual ESRI International Conference, San Diego, California, USA*.

Camporeale, C., Perucca, E., & Ridolfi, L. (2008). Significance of cutoff in meandering river dynamics. *Journal of Geophysical Research: Earth Surface*, *113*, n/a–n/a. URL: http://dx.doi.org/10.1029/2006JF000694. doi:10.1029/2006JF000694. F01001.

Carling, P., Jansen, J., & Meshkova, L. (2014). Multichannel rivers: their definition and classification. *Earth Surface Processes and Landforms*, *39*, 26–37. URL: http://dx.doi.org/10.1002/esp.3419. doi:10.1002/esp.3419.

Carlson, T. N., & Riziley, D. A. (1997). On the relation between ndvi, fractional vegetation cover, and leaf area index. *Remote Sensing of Environment*, *62*, 241–252.

Choi, W., Lam, K., & Siu, W. (2003). Extraction of the euclidean skeleton based on a connectivity criterion. *Pattern Recognition*, *36*, 721–729.

Colombini, M., Seminara, G., & Tubino, M. (1987). Finite-amplitude alternate bars. *Journal of Fluid Mechanics*, *181*, 213–232.

Constantine, J. A. (2006). *Quantifying the Connections Between Flow, Bar Deposition, and Meander Migration in Large Gravel-Bed Rivers*. Ph.D. thesis University of California.

Constantine, J. A., Dunne, T., Ahmed, J., Legleiter, C., & Lazarus, E. D. (2014). Sediment supply as a driver of river meandering and floodplain evolution in the amazon basin. *Nature Geoscience*, *7*, 899.

Constantine, J. A., McLean, S. R., & Dunne, T. (2009). A mechanism of chute cutoff along large meandering rivers with uniform floodplain topography. *Geological Society of America Bul-*

letin, *122*, 855–869. URL: http://gsabulletin.gsapubs.org/cgi/doi/10.1130/B26560.1. doi:10.1130/B26560.1.

Constantine, J. A., McLean, S. R., & Dunne, T. (2010). A mechanism of chute cutoff along large meandering rivers with uniform floodplain topography. *Geological Society of America Bulletin*, *122*, 855–869.

Dey, A., & Bhattacharya, R. (2013). Monitoring of river center line and width–a study on river brahmaputra. *Journal of the Indian Society of Remote Sensing*, (pp. 1–8).

Edwards, B. F., & Smith, D. H. (2002). River meandering dynamics. *Phys. Rev. E*, *65*, 046303. URL: http://link.aps.org/doi/10.1103/PhysRevE.65.046303. doi:10.1103/PhysRevE.65.046303.

Eke, E. C. (2013). *Numerical Modeling of River Migration incorporating erosional and depositional bank processes*. Ph.D. thesis University of Illinois at Urbana-Champaign.

Eke, E. C., Czapiga, M. J., Viparelli, E., Shimizu, Y., Imran, J., Sun, T., & Parker, G. (2014a). Coevolution of width and sinuosity in meandering rivers. *Journal of Fluid Mechanics*, *760*, 127–174. doi:10.1017/jfm.2014.556.

Eke, E. C., Parker, G., & Shimizu, Y. (2014b). Numerical modeling of erosional and depositional bank processes in migrating river bends with self-formed width: Morphodynamics of bar push and bank pull. *Journal of Geophysical Research*, *119*, 1455–1483. doi:10.1002/2013JF003020.Received.

Feyisa, G. L., H., M., R., F., & Proud, S. R. (2014). Automated water extraction index: A new technique for surface water mapping using landsat imagery. *Remote Sensing of Environment*, *140*, 23–35.

Fisher, G. B., Bookhagen, B., & Amos, C. B. (2013). Channel planform geometry and slopes from freely available high-spatial resolution imagery and dem fusion: implications for channel width scalings, erosion proxies, and fluvial signatures in tectonically active landscapes. *Geomorphology*, *194*, 46–56.

Fuller, I. C., Large, A. R., Charlton, M. E., Heritage, G. L., & Milan, D. J. (2003). Reach-scale sediment transfers: An evaluation of two morphological budgeting approaches. *Earth Surface Processes and Landforms*, *8*, 889–903.

Gao, B. (1996). Ndwi a normalized difference water index for remote sensing of vegetation liquid water from space. *Remote Sensing of Environment*, *58*, 257–266.

Gittins, S. (2004). *Exposed river sediment dynamic on Welsh rivers*. Ph.D. thesis.

Güneralp, I., Filippi, A. M., & Hales, B. (2014). Influence of river channel morphology and bank characteristics on water surface boundary delineation using high-resolution passive remote sensing and template matching. *Earth Surface Processes and Landforms*, *39*, 977–986. URL: http://dx.doi.org/10.1002/esp.3560. doi:10.1002/esp.3560. ESP-13-0265.R1.

Güneralp, I., Filippi, A. M., & Hales, B. U. (2013). River-flow boundary delineation from digital aerial photography and ancillary images using support vector machines. *GIScience & Remote Sensing*, *50*, 1–25.

Güneralp, I., & Rhoads, B. L. (2007). Continuous Characterization of the Planform Geometry and Curvature of Meandering Rivers. *Geographical Analysis*, *40*, 1–25.

Güneralp, I., & Rhoads, B. L. (2009). Empirical analysis of the planform curvature-migration relation of meandering rivers. *Water Resources Research*, *45*.

Güneralp, I., & Rhoads, B. L. (2011). Influence of floodplain erosional heterogeneity on planform complexity of meandering rivers. *Geophysical Research Letters*, *38*. URL: http://doi.wiley.com/10.1029/2011GL048134. doi:10.1029/2011GL048134.

Haralick, R. M., Sternberg, S. R., & Zhuang, X. (1987). Image analysis using mathematical morphology. *IEEE transactions on pattern analysis and machine intelligence*, (pp. 532–550).

Henshaw, A. J., Gurnell, A., Bertoldi, W., & Drake, N. A. (2013). An assessment of the degree to which landsat {TM} data can support the assessment of fluvial dynamics, as revealed by changes in vegetation extent and channel position, along a large river. *Geomorphology*, *202*, 74 – 85. URL: http://www.sciencedirect.com/science/article/pii/S0169555X1300038X. doi:http://dx.doi.org/10.1016/j.geomorph.2013.01.011. Process geomorphology and ecosystems: Disturbance regimes and interactions.

Hooke, J. M. (2003). River meander behaviour and instability. *Royal Geography Society*, (pp. 238–253).

Hooke, J. M. (2004). Cutoff galore!: occurrence and causes of multiple cutoffs on a meandering river. *Geomorphology*, (pp. 225–238). doi:10.1016/j.geomorph.2003.12.006.

Hooke, J. M. (2007). Spatial Variability, mechanisms and propagation of change in an active meandering river. *Geomorphology*, *84*, 277–296.

Hooke, J. M., Gautier, E., & Zolezzi, G. (2011). River meander dynamics: developments in modelling and empirical analyses. *Earth Surface Processes and Landforms*, *36*, 1550–1553.

961 URL: http://doi.wiley.com/10.1002/esp.2185. doi:10.1002/esp.2185.
962 Hooke, J. M., & Yorke, L. (2011). Channel bar dynamics on multi-decadal timescales in an
963 active meandering river. *Earth Surface Processes and Landforms*, *36*, 1910–1928.
964 Howard, A. D. (1992). Modeling channel migration and floodplain sedimentation in meandering
965 streams. *Lowland Floodplain Rivers: Geomorphological Perspectives*, (pp. 1–41).
966 Ikeda, S., Parker, G., & Sawai, K. (1981). Bend theory of river meanders. part 1. linear devel-
967 opment. *Journal of Fluid Mechanics*, *112*. doi:10.1017/S0022112081000451.
968 Isikdogan, F., Bovik, A., & Passalacqua, P. (2017). RivaMap: An automated river analysis and
969 mapping engine. *Remote Sensing of Environment*, *202*, 88–97.
970 Johannesson, H., & Parker, G. (1989). Linear theory of river meanders. *American Geophysical*
971 *Union*, . doi:10.1029/WM012p0181.
972 Jones, E., Oliphant, T., Peterson, P. et al. (2001). SciPy: Open source scientific tools for Python.
973 URL: http://www.scipy.org/ [Online; accessed ¡today¿].
974 Kasvi, E., Vaaja, M., Alho, P., Hyyppä, H., Hyyppä, J., Kaartinen, H., & Kukko, A. (2013).
975 Morphological changes on meander point bars associated with flow structure at different
976 discharges. *Earth Surface Processes and Landforms*, *38*, 577–590. URL: http://doi.wiley.
977 com/10.1002/esp.3303. doi:10.1002/esp.3303.
978 Kinoshita, R. (1961). *Investigation of channel deformation in Ishikari River*. Technical Report
979 36 Nat. Resour. Div., Minist. of Sci. and Technol. of Jpn.
980 Kinoshita, R., & Miwa, H. (1974). River channel formation which prevents downstream trans-
981 lation of transverse bars. *Shinsabo*, (pp. 12–17 (in japanese)).
982 Kleinhans, M. G., & van den Berg, J. H. (2011). River channel and bar patterns explained and
983 predicted by an empirical and a physics-based method. *Earth Surf. Processes Landforms*, *6*,
984 721–738. doi:10.1002/esp.2090.
985 van de Lageweg, W. I., van Dijk, W. M., Baar, A. W., Rutten, J., & Kleinhans, M. G. (2014).
986 Bank pull or bar push: What drives scroll-bar formation in meandering rivers? *Geology*, *42*,
987 319–322.
988 Latrubesse, E. M. (2008). Patterns of anabranching channels: The ultimate end-member adjust-
989 ment of mega rivers. *Geomorphology*, *101*, 130 – 145. URL: http://www.sciencedirect.com/
990 science/article/pii/S0169555X08002389. doi:http://dx.doi.org/10.1016/j.geomorph.
991 2008.05.035. The 39th Annual Binghamton Geomorphology Symposium: Fluvial Deposits

and Environmental History: Geoarchaeology, Paleohydrology, and Adjustment to Environmental Change.

Latrubesse, E. M., Amsler, M. L., de Morais, R. P., & Aquino, S. (2009). The geomorphologic response of a large pristine alluvial river to tremendous deforestation in the south american tropics: The case of the araguaia river. *Geomorphology*, *113*, 239 – 252. URL: http://www.sciencedirect.com/science/article/pii/S0169555X09001238. doi:http://dx.doi.org/10.1016/j.geomorph.2009.03.014. Short and Long Term Processes, Landforms and Responses in Large Rivers.

Lauer, J. W. (2006). *NCED Stream Restoration Toolbox - Channel Planform Statistics*. National Center for Earth-Surface Dynamics.

Lauer, J. W., & Parker, G. (2008). Net local removal of floodplain sediment by river meander migration. *Geomorphology*, *96*, 123–149.

Legleiter, C. J., Harrison, L. R., & Dunne, T. (2011). Effect of point bar development on the local force balance governing flow in a simple, meandering gravel bed river. *Journal of Geophysical Research*, *116*, F01005. URL: http://doi.wiley.com/10.1029/2010JF001838. doi:10.1029/2010JF001838.

Legleiter, C. J., & Kyriakidis, P. C. (2006). Forward and inverse transformations between cartesian and channel-fitted coordinate systems for meandering rivers. *Mathematical Geology*, *38*, 927–958. URL: http://dx.doi.org/10.1007/s11004-006-9056-6. doi:10.1007/s11004-006-9056-6.

Leopold, L. B., & Wolman, G. M. (1960). River meanders. *Bulletin of Geological Society of America*, *71*, 769–794.

Lewin, J. (1972). Late-stage meander growth. *Nature*, *240*, 116–116.

Lewin, J., & Brewer, P. A. (2001). Predicting channel patterns. *Geomorphology*, *40*, 329–339. doi:10.1016/S0169-555X(01)00061-7.

Lu, S., Wu, B., Yan, N., & Wang, H. (2011). Water body mapping method with hj-1a/b satellite imagery. *International Journal of Applied Earth Observation and Geoinformation*, *13*, 428 – 434. URL: http://www.sciencedirect.com/science/article/pii/S0303243410001108. doi:http://dx.doi.org/10.1016/j.jag.2010.09.006.

Luchi, R., Hooke, J. M., Zolezzi, G., & Bertoldi, W. (2010a). Width variations and mid-channel bar inception in meanders: River Bollin (UK). *Geomorphology*, *119*, 1–8.

URL: http://linkinghub.elsevier.com/retrieve/pii/S0169555X1000036X. doi:10.1016/j.geomorph.2010.01.010.

Luchi, R., Zolezzi, G., & Tubino, M. (2010b). Modelling mid-channel bars in meandering channels. *Earth Surface Processes and Landforms*, *35*, 902–917. URL: http://doi.wiley.com/10.1002/esp.1947. doi:10.1002/esp.1947.

Luchi, R., Zolezzi, G., & Tubino, M. (2011). Bend theory of river meanders with spatial width variations. *Journal of Fluid Mechanics*, *681*, 311–339. URL: http://www.journals.cambridge.org/abstract_S002211201100200X. doi:10.1017/jfm.2011.200.

Merwade, V. M. (2007). An automated gis procedure for delineating river and lake boundaries. *Transactions in GIS*, *11*, 213–231. URL: http://dx.doi.org/10.1111/j.1467-9671.2007.01042.x. doi:10.1111/j.1467-9671.2007.01042.x.

Merwade, V. M., Maidment, D. R., & Hodges, B. R. (2005). Geospatial representation of river channels. *Journal of Hydrologic Engineering*, *10*, 243–251. doi:10.1061/(ASCE)1084-0699(2005)10:3(243).

Mosselman, E. (1998). Morphological modelling of rivers with erodible banks. *Hydrological processes*, *12*, 1357–1370.

Motta, D., Abad, J. D., & Garcia, M. H. (2012). A simplified 2d model for meander migration with physically-based bank evolution. *Geomorphology*, *163-164*, 10–25.

Nanson, G. C., & Hickin, E. J. (1983). Channel Migration and Incision in the Beatton River. *J. Hydraul. Eng.*, *109*, 327–337.

Nanson, G. C., & Knighton, A. D. (1996). Anabranching rivers: their cause, character and classification. *Earth Surface Processes and Landforms*, *21*, 217–239. URL: http://dx.doi.org/10.1002/(SICI)1096-9837(199603)21:3<217::AID-ESP611>3.0.CO;2-U. doi:10.1002/(SICI)1096-9837(199603)21:3<217::AID-ESP611>3.0.CO;2-U.

Ninomiya, Y. (2004). Lithologic mapping with multispectral aster tir and swir data. In *Proc. SPIE* (pp. 180–190). volume 5234. URL: http://dx.doi.org/10.1117/12.511902. doi:10.1117/12.511902.

O'Callaghan, M. J., Hannah, D. M., Williams, M., & Sadler, J. P. (2013). Exposed riverine sediments (ers) in england and wales: distribution, controls and management. *Aquatic Conservation: Marine and Freshwater Ecosystems*, *23*, 924–938.

Oliphant, T. E. (2006). *A guide to NumPy* volume 1. Trelgol Publishing USA.

Otsu, N. (1979). A threshold selection method from gray-level histograms. *IEEE Trans. Sys., Man., Cyber.*, *9*, 62–66. doi:doi:10.1109/TSMC.1979.4310076.

Pai, N., & Saraswat, D. (2013). A geospatial tool for delineating streambanks. *Environmental Modelling & Software*, *40*, 151–159. URL: https://www.sciencedirect.com/science/article/pii/S1364815212002344. doi:10.1016/J.ENVSOFT.2012.08.012.

Pavelsky, T. M., & Smith, L. C. (2008). RivWidth: A Software Tool for the Calculation of River Widths From Remotely Sensed Imagery. *IEEE Geoscience and Remote Sensing Letters*, *5*, 70–73. doi:10.1109/LGRS.2007.908305.

Peixoto, J., Nelson, B., & Wittmann, F. (2009). Spatial and temporal dynamics of river channel migration and vegetation in central amazonian white-water floodplains by remote-sensing techniques. *Remote Sens. Environ.*, *113*, 2258–2266.

Rowland, J. C., Shelef, E., Pope, P. A., Muss, J., Gangodagamage, C., Brumby, S. P., & Wilson, C. J. (2016). A morphology independent methodology for quantifying planview river change and characteristics from remotely sensed imagery. *Remote Sensing of Environment*, *184*, 212 – 228. URL: http://www.sciencedirect.com/science/article/pii/S0034425716302620. doi:http://dx.doi.org/10.1016/j.rse.2016.07.005.

Sangireddy, H., Stark, C. P., Kladzyk, A., & Passalacqua, P. (2016). GeoNet: An open source software for the automatic and objective extraction of channel heads, channel network, and channel morphology from high resolution topography data. *Environmental Modelling & Software*, *83*, 58–73. URL: https://www.sciencedirect.com/science/article/pii/S1364815216301219. doi:10.1016/J.ENVSOFT.2016.04.026.

Schuurman, F., Shimizu, Y., Iwasaki, T., & Kleinhans, M. G. (2016). Dynamic meandering in response to upstream perturbations and floodplain formation. *Geomorphology*, *253*, 94–109. URL: http://www.sciencedirect.com/science/article/pii/S0169555X15003815. doi:http://dx.doi.org/10.1016/j.geomorph.2015.05.039.

Schwendel, A. C., Nicholas, A. P., Aalto, R. E., H., S. S. G., & Buckley, S. (2015). Interaction between meander dynamics and floodplain heterogeneity in a large tropical sand-bed river: the rio beni, bolivian amazon. *Earth Surf. Process. Landforms*, . doi:10.1002/esp.3777.

Schwenk, J., & Foufoula-Georgiou, E. (2015). Accelerated migration rates downstream of a human-induced cutoff in the ucayali river, peru. In *9th Symposium of River, Coastal and Estuarine Morphodynamics*.

Schwenk, J., & Foufoula-Georgiou, E. (2016). Meander cutoffs nonlocally accelerate upstream and downstream migration and channel widening. *Geophysical Research Letters*, *43*, 12,437–12,445. doi:10.1002/2016GL071670.

Schwenk, J., Khandelwal, A., Fratkin, M., Kumar, V., & Foufoula-Georgiou, E. (2016). High spatio-temporal resolution of river planform dynamics from landsat: the rivmap toolbox and results from the ucayali river. *Earth and Space Science*, (pp. n/a–n/a). URL: http://dx.doi.org/10.1002/2016EA000196. doi:10.1002/2016EA000196. 2016EA000196.

Schwenk, J., Lanzoni, S., & Foufoula-Georgiou, E. (2015). The life of a meander bend: Connecting shape and dynamics via analysis of a numerical model. *J. Geophys.Res. Earth Surf.*, *120*, 690–710. doi:10.1002/2014JF003252.

Seminara, G. (2006). Meanders. *Journal of fluid mechanics*, *554*, 271–297. doi:10.1017/S0022112006008925.

Seminara, G., Zolezzi, G., Tubino, M., & Zardi, D. (2001). Downstream and upstream influence in river meandering. Part 2. Planimetric development. *Journal of Fluid Mechanics*, *438*, 213–230.

Serra, J. (1982). *Image analysis and mathematical morphology, v. 1*. Academic press.

Serra, J. (1986). Introduction to mathematical morphology. *Computer vision, graphics, and image processing*, *35*, 283–305.

Smith, J. D., & Mclean, S. R. (1984). A model for flow in meandering streams. *Water Resources Research*, *20*, 1301–1315. URL: http://dx.doi.org/10.1029/WR020i009p01301. doi:10.1029/WR020i009p01301.

Song, C., Woodcock, C. E., Seto, K. C., Lenney, M. P., & Macomber, S. A. (2001). Classification and change detection using landsat tm data: when and how to correct atmospheric effects? *Remote sensing of Environment*, *2*, 230–244.

Subramaniam, S., Suresh Babu, A. V., & S., R. P. (2011). Automated water spread mapping using resourcesat-1 awifs data for water bodies information system. *IEEE Journal of Selected Topics in Applied Earth Observations and Remote Sensing*, *4*, 205–215. doi:10.1109/JSTARS.2010.2085032.

Sun, T., Meakin, P., Jossang, T., & Schwarz, K. (1996). A simulation model for meandering rivers. *Water Resources Research*, *32*, 2937–2954. URL: http://dx.doi.org/10.1029/96WR00998. doi:10.1029/96WR00998.

Tubino, M. (1991). Growth of alternate bars in unsteady flow. *Water Resources Research*, *27*, 37–52. URL: http://dx.doi.org/10.1029/90WR01699. doi:10.1029/90WR01699.

Tubino, M., & Seminara, G. (1990). Free–forced interactions in developing meanders and suppression of free bars. *Journal of Fluid Mechanics*, *214*, 131–159. URL: http://journals.cambridge.org/article_S0022112090000088. doi:10.1017/S0022112090000088.

Van der Walt, S., Schönberger, J. L., Nunez-Iglesias, J., Boulogne, F., Warner, J. D., Yager, N., Gouillart, E., & Yu, T. (2014). scikit-image: image processing in python. *PeerJ*, *2*, e453.

Xu, H. (2005). A study on information extraction of water body with the modified normalized difference water index (mndwi). *Journal of Remote Sensing*, *5*, 589–595.

Xu, H. (2006). Modification of normalised difference water index (ndwi) to enhance open water features in remotely sensed imagery. *International Journal of Remote Sensing*, *27*, 3025–3033.

Zhang, T. Y., & Suen, C. Y. (1984). A fast parallel algorithm for thinning digital patterns. *Communications of the ACM*, *27*, 236–239.

Zolezzi, G., Bertoldi, W., & Tubino, M. (2012). Morphodynamics of bars in gravel-bed rivers: Bridging analytical models and field observations. *Gravel-Bed Rivers: Processes, Tools, Environments*, (pp. 69–89).

Zolezzi, G., & Seminara, G. (2001). Downstream and upstream influence in river meandering. part 1. general theory and application to overdeepening. *Journal of Fluid Mechanics*, *438*, 183–211. URL: http://journals.cambridge.org/article_S002211200100427X. doi:10.1017/S002211200100427X.